CENTER FOR INFRASTRUCTURE ENGINEERING STUDIES

FRP Jacketed Reinforced Concrete Columns

by

Chris Cole

Abdeldjelil Belarbi

Department of Civil Engineering

University of Missouri - Rolla

May 2001

CIES 99-13

Disclaimer

The contents of this report reflect the views of the author(s), who are responsible for the facts and the accuracy of information presented herein. This document is disseminated under the sponsorship of the Center for Infrastructure Engineering Studies (CIES), University of Missouri -Rolla, in the interest of information exchange. CIES assumes no liability for the contents or use thereof.

The mission of CIES is to provide leadership in research and education for solving society's problems affecting the nation's infrastructure systems. CIES is the primary conduit for communication among those on the UMR campus interested in infrastructure studies and provides coordination for collaborative efforts. CIES activities include interdisciplinary research and development with projects tailored to address needs of federal agencies, state agencies, and private industry as well as technology transfer and continuing/distance education to the engineering community and industry.

Center for Infrastructure Engineering Studies (CIES)
University of Missouri-Rolla
223 Engineering Research Lab
1870 Miner Circle
Rolla, MO 65409-0710
Tel: (573) 341-6223; fax -6215
E-mail: cies@umr.edu
www.cies.umr.edu

ABSTRACT

Previous research has established that retrofitting RC (reinforced concrete) columns with FRP (fiber reinforced polymer) jackets is an effective means of providing external confinement to the column cross section. In an effort to further FRP jacketing technology, this study focused on the confinement effectiveness of FRP jackets for rectangular building-type RC columns. Twenty-six fourth-scale short columns were tested to failure in axial compression. Variables investigated include the following: the type of fibers (AFRP, CFRP, or GFRP), the thickness of the jacket, the shape (rectangular or circular) and aspect ratio of the cross section, the amount of longitudinal steel reinforcement, the spacing of the transverse steel reinforcement, and the sharpness of the corners of the rectangular cross sections. Unjacketed columns were included in the testing matrix for reference. The specimens were instrumented to measure axial deformation, as well as the distribution of the hoop strain in the jackets. For square columns, GFRP jackets were observed to increase the ultimate axial strain more effectively than either AFRP or CFRP jackets. For multiple-ply jackets on square columns, GFRP was also found to be the most effective at increasing the ultimate axial normalized stress. Increasing the aspect ratio of the rectangular cross sections resulted in a decrease in confinement effectiveness, as did increasing the sharpness of the corners. The ultimate axial stresses sustained by the jacketed specimens were compared to the predictions of a model from the literature. The agreement between the model and the experimental results varied widely, but on the average the model overestimated the strength of the columns by about 14%.

TABLE OF CONTENTS

Page

LIST OF ILLUSTRATIONS

Page

LIST OF TABLES

Page

LIST OF ABBREVIATIONS

A_c	Area of concrete within a cross section
A_e	Effective area of confined concrete
A_s	Area of longitudinal steel within a cross section
D	Diameter of a circular cross section
E_c	Elastic modulus of concrete
E_j	Elastic modulus of jacket fibers
E_n	Slope of the elastic portion of the normalized stress versus deformation curve
f'_c	Compressive strength of concrete
f_{cc}	Compressive strength of FRP-confined concrete
f_{cz}	Compressive stress in FRP-confined concrete (Xiao and Wu, 2000)
f_r	Lateral confining pressure
$f_{r,x}$	Effective lateral confining pressure in the x direction for rectangular cross sections
$f_{r,y}$	Effective lateral confining pressure in the y direction for rectangular cross sections
f_s	Stress in reinforcing steel
f_y	Yield strength of reinforcing steel
P	Axial load applied to a test specimen at a given load stage
P_{ult}	Maximum axial load applied to a test specimen
t_j	Thickness of FRP jacket
t_x	Length of rectangular cross section in the x direction
t_y	Length of rectangular cross section in the y direction
W_x	That portion of the x dimension of a rectangular cross section between the corner radii (see Figure 4.38)
W_y	That portion of the y dimension of a rectangular cross section between the corner radii (see Figure 4.38)
α, k	Experimentally determined coefficients used to quantify f_{cz}
ε_c	Axial strain in concrete

ε_j Axial strain in jacket fibers

σ_c Stress in concrete

$\sigma_{n,ult}$ Maximum normalized concrete stress

1. INTRODUCTION

1.1. GENERAL

Existing reinforced concrete (RC) structures may require strengthening for a variety of reasons. For example, it is often desirable to increase the loading to which a structure is subjected, as when a bridge must carry increased traffic or when a building must be used for purposes other than those for which it was originally designed. It may also be necessary to strengthen old RC structures as a result of new code requirements or because of damage to the structure as a result of environmental stresses.

Within the framework of the general problem of strengthening RC structures, there exists the issue of strengthening RC columns. The strengthening of RC columns represents an engineering problem, which, like all engineering problems, involves several solutions, each having its own advantages and disadvantages and its own limits to its applicability and practicality. For instance, it is possible to remove deficient columns and construct new ones in their place. Another solution is to place reinforcing steel and formwork around a column and pour additional concrete (Picher et al. 1996). Yet another solution is to use a jacketing scheme wherein the column is encased by some reinforcing material. Traditionally, steel has been used to jacket RC columns, but recently fiber reinforced polymer (FRP) has become a viable alternative to steel in some applications. This study will focus on the use of FRP as a jacketing material.

1.2. FRP COMPOSITES

FRP is an advanced composite material that is relatively new to civil infrastructure engineering. It holds promise to be a better choice than steel in certain applications. One of its most significant advantages is that it is a lightweight material, which makes its installation costs low in comparison to steel. FRP is also more easily negotiated into spatially restrictive areas than steel and is much more resistant to corrosion. FRP has been used in aerospace and military applications for decades, principally because of its high strength to weight ratio, but traditionally has not been available as a structural

material for civil engineering projects because of its high cost. Technological advances in the past several years, however, have made FRP practical for use as a building material. Consequently, it is being studied extensively in order to identify and overcome the technical hurdles associated with its use.

FRP is composed of high strength, high modulus synthetic fibers embedded in a polymer material. While the polymer has little load carrying capacity itself, it does serve the important functions of holding the fibers in place, protecting the fibers from chemical, UV and mechanical damage, and serving as a vehicle through which external loads are applied to the fibers (Mallick 1988). The fibers, being the main load-carrying constituent, give FRP its strength. For civil engineering applications, the types of fibers commonly used are glass, carbon, and aramid. The fibers are anisotropic - that is, their mechanical properties vary based on the axis along which the properties are measured. Table 1.1 displays the properties associated with tensile loading along the longitudinal axis of the fibers for the three types of fibers that are generally used in civil infrastructure engineering and hence, in this study. All of the fibers exhibit linear elastic behavior until brittle fracture occurs at their respective ultimate stresses.

Table 1.1. Mechanical Properties of High Strength Fibers

Fiber Type	Guaranteed Ultimate Strength (MPa)	Elastic Modulus (GPa)
CF 130 High Tensile Carbon	3,790	228
AK 60 Aramid	2,000	117
EG 900 E-Glass	1,520	72.4

As one might expect, carbon, aramid, and glass fibers have both similarities and differences. All three are subject to a phenomenon known as creep rupture; that is, failure that occurs under sustained loading at stresses less than the ultimate tensile stress suggested by a standard short-term (lasting only a few minutes) tension test. Carbon is most resistant to creep rupture, while glass is most susceptible (Slattery 1994) and will

eventually fail if the applied load is greater than about 30% of its ultimate short-term tensile strength (MBrace™ 1998). The three types of fibers exhibit varying levels of resistance to freeze-thaw and wet-dry cycles, carbon being the most resistant and glass being the most susceptible (Chajes et al. 1994) (tests done in the presence of chlorides). In addition, glass has the advantages of being low cost and an insulator and the disadvantages of having a low modulus of elasticity and sensitivity to abrasion and moisture. Carbon has a low coefficient of thermal expansion but also has low electrical resistance. Aramid is resistant to damage caused by dynamic loading but is UV sensitive and has a low compressive strength (Mallick 1988).

1.3. FRP JACKETS ON RC COLUMNS

Jacketing an RC column with FRP primarily improves column performance, not because the jacket itself carries some fraction of the axial load applied to the column, but rather because it provides lateral confining pressure to the column. This confining pressure places the concrete in a triaxial state of stress, altering the load-deformation characteristics of the concrete. High levels of confining pressure enable concrete to sustain both greater axial loads and greater ultimate axial strain by changing the failure mode from cleavage of the concrete to the crushing of its cement paste (Chen 1982). FRP jackets can apply confining pressure either actively or passively. In the active retrofit scheme the fibers are tensioned either as they are wrapped around the column or by pressure injecting grout or epoxy between the jacket and the column. In the passive scheme, the confining pressure is a result of the reaction of the jacket against the lateral dilation of the column cross section as it is loaded axially.

In the case of a circular cross section, the jacket exerts a uniform confining pressure resulting in a uniform triaxial stress field. In a non-circular cross section, the confinement results in a complex non-uniform triaxial stress field, which generally results in a lower level of performance in comparison to circular cross sections.

1.4. PROBLEM DEFINITION

Thus far, the main thrust of research involving FRP-jacketed columns has been aimed at characterizing the behavior of columns with circular cross sections. The results of such research have wide applicability, particularly with regard to circular bridge piers. However, the vast majority of all columns in buildings are rectangular columns. Therefore, their strengthening and rehabilitation need to be given attention to preserve the integrity of building infrastructure. This experimental study focused on the passive retrofit scheme applied to non-slender columns under pure axial compression. The objective was to determine the effect of various experimental parameters on the confinement effectiveness of FRP jackets on rectangular columns. These experimental parameters included the cross-sectional aspect ratio (the ratio of the length of the long side of the cross section to that of the short side) of the column, the amount and type of fibers constituting the FRP jacket, the sharpness of the column corners, and the amount of longitudinal and transverse steel reinforcement in the column. The unconfined cylinder strength of the concrete was held approximately constant for all columns.

1.5. ORGANIZATION OF THE REPORT

Four sections proceed this introductory section. Section 2 summarizes existing literature on the strengthening of RC columns with FRP jackets. Section 3 describes in detail the experimental program undertaken in this study, including a description of the specimens and the manner in which they were constructed, instrumented and tested. Section 4 presents the results of the testing program. Lastly, Section 5 lists the conclusions drawn from the study.

2. LITERATURE REVIEW

2.1. INTRODUCTION

The purpose of this section is to relate what is already known about the behavior of FRP-confined concrete by discussing the theoretical derivations and experimental findings of previous studies. In the literature, two primary areas of research related to columns have been pursued: One area concerns the effect of FRP confinement on RC beam-columns subjected to both axial loads and bending moments. The other area focuses on quantifying and understanding the stress-strain behavior of plain FRP-confined concrete under axial compression. Both areas will be reviewed in this section, however the latter will be given greater attention, as it is more pertinent to the current study.

In the literature, certain terms frequently arise in the description of test specimens composed of FRP-confined concrete. For instance, specimens may be referred to as bonded or unbonded. The bond is in reference to the interface between the concrete and the FRP. The FRP in bonded specimens is firmly attached to the concrete, either mechanically or adhesively. In unbonded specimens, little more than friction joins the concrete to the FRP.

There are many ways in which columns can be confined with FRP. One method is to use prefabricated FRP shells, straps or tubes. Shells and straps are preformed sheets or belts of FRP made to fit a particular column geometry. Tubes are hollow FRP members that can initially function as formwork for the column (Saafi et al. 1999). After the concrete is poured and has cured, then the tube remains in place and acts as a structural part of the column. Another method is to saturate sheets of dry fiber with resin and apply them to the column. Once the resin has cured, the jacket is fully functional. One benefit of this method is that the sheets can be formed into a wide variety of shapes on-site. Yet another method, filament winding, is similar to using sheets, except that strands of fibers saturated with resin are used to form the jacket. Filament winding is typically done with a machine. Some investigators have used filament winding to wind FRP directly onto

their specimens, while others use this technique in conjunction with molds to make prefabricated FRP shapes.

In this study, FRP applied to a column after the concrete has cured will be referred to as a jacket. FRP that acts as formwork for a column will be referred to as a tube. As a result of the nature of the method of construction, jackets are generally bonded to the concrete they encase, while tubes are unbonded. However, as will be discussed later, there are methods for constructing unbonded jackets and bonded tubes.

Since the properties of FRP are heavily directionally dependent, researchers usually describe the orientation of the fibers on their FRP-confined test specimens. In this study, the fiber orientation will be described with reference to the longitudinal axis of the column. For instance, a 90-degree fiber orientation indicates that the fibers in the FRP are perpendicular to the long axis of the column. The notation for more complex geometries will be described later in the section.

2.2. FRP-CONFINED BEAM-COLUMNS

Reinforced concrete columns constructed in accordance with pre-1970's design codes can have structural deficiencies (Saadatmanesh et al. 1993; Saadatmanesh 1997; Xiao et al. 1999), particularly with regard to their performance in seismic events. Some of the common flaws include the following:

- Transverse hoop development – Hoops are developed in the cover, which may cause a loss of anchorage in the event of spalling.
- Lap length in reinforcement splicing details – Lap lengths for the starter bars at the column/foundation interface are not sufficient to develop the yield strength of the bars, which can result in a brittle bond failure.
- Amount of transverse reinforcement – The amount of transverse reinforcement included in the columns is not sufficient.

Research, as discussed below, has shown that retrofitting columns with FRP jackets can significantly improve the performance of these columns.

Xiao et al. (1999) investigated the use of FRP jackets for improving the shear strength of circular columns. Their research was targeted at existing pre-1970's columns whose shear strengths were less than their flexural strengths. The objective of the research was thus to increase the shear strength of the columns in order to force a ductile flexural mode of failure. Their goal was to attain a maximum displacement ductility ratio greater than six, where the displacement ductility ratio is defined as the lateral displacement of the column divided by the lateral displacement of the column at first yield of longitudinal steel. Three test specimens 2.44 m tall and 610 mm in diameter were constructed to model the deficient columns.

One specimen was tested unretrofitted, while the other two were jacketed along their entire length using prefabricated composite shells composed of unidirectional glass fibers and a polyester resin. The shells were bonded to the specimens at a 90-degree fiber orientation using a urethane adhesive. The loading of the specimens during testing subjected them to double curvature under a constant axial load and a cyclic (alternately pushing and pulling) lateral load, much like a column might experience in an actual seismic event.

As expected, the unjacketed column failed in a somewhat brittle flexural/shear mode. It achieved a maximum displacement ductility ratio of three. The performance of the jacketed columns showed marked improvement, maintaining stable response to displacement ductility levels of fourteen. In addition, the investigators noted that the stiffnesses of the jacketed columns were not significantly increased by the retrofit. This is in contrast to steel jackets that do, in fact, increase the stiffness of the columns, causing them to attract additional earthquake loads.

As part of their research efforts, the authors also investigated the installation benefits of this particular composite retrofit technique in the field. As it turned out, approximately two hours with a three-member crew and a hydraulic platform was sufficient to apply a four-layer shell jacket on a column 8 m tall and 914 mm in diameter. They stated that a

similar steel retrofit would have taken three to four days, as well as labor from different trades and more heavy equipment.

Saadatmanesh (1997) performed tests on $^1/_5$-scale circular and rectangular RC columns having footings with insufficient lap length in the starter bars. As shown in Figure 2.1, the specimens were bolted through their footings during testing as constant axial load and cyclic lateral loads were applied. The jacketed columns in the test matrix were fitted with GFRP straps at a 90-degree fiber orientation in the potential plastic hinge region (see Figure 2.1). In addition, the jacketed square columns were also injected with pressurized epoxy at 550 kPa between the face of the columns and the straps to enhance confinement.

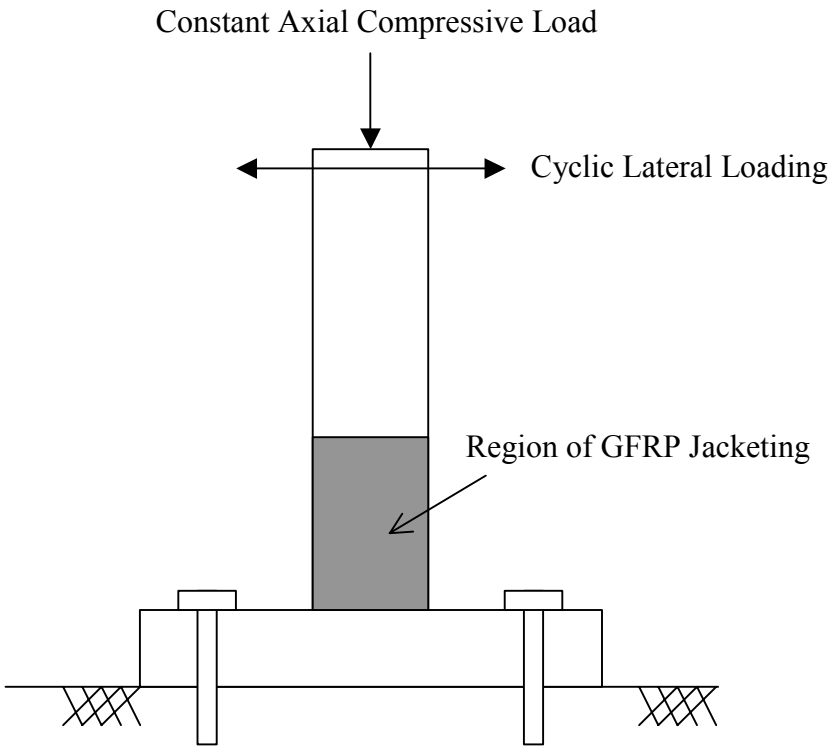

Figure 2.1. Test Specimen and Loading Configuration
for Tests Performed by Saadatmanesh (1997)

During testing, the lateral load capacity of the unjacketed circular column dropped rapidly after a displacement ductility of about 1.5. The failure mode was noted to be debonding of the longitudinal reinforcement near the column/footing interface. A similar jacketed column sustained a displacement ductility level of six with no sign of bond failure and carried a maximum lateral load 40% greater than its unjacketed counterpart.

After loading the unjacketed columns to complete failure, a repair technique was investigated. The loose concrete around the failure region was chipped away and new concrete was poured to restore the cross sections to their original dimensions. The repaired columns were then jacketed with GFRP straps and retested. For both rectangular and circular cross sections, the repaired columns performed better than in their original unjacketed condition.

Pantelides et al. (1999) took advantage of an opportunity to bring their research out of the lab and into the field during the recent reconstruction of Interstate 15. The researchers were given the opportunity to test two bridge piers before their scheduled demolition. Both piers were part of the same bridge and each consisted of three square columns joined by a pier cap. They were tested by applying cyclic lateral loads in plane with their frames, while half of the original dead load of the bridge deck acted. CFRP sheets were applied to the columns to confine the flexural plastic hinges, to shear strengthen the columns and to clamp the lap splice regions near the footings. CFRP was also applied to the bent. The goal of the retrofit was to double the displacement ductility of the pier. This goal was achieved. In addition, the lateral load capacity was increased by 16%.

A final point on the confinement effectiveness of composite jackets on beam-columns is noteworthy. The research that is discussed in the following paragraphs shows clearly that composite jackets can significantly increase the ultimate axial stress and axial strain of concrete placed in uniform compression. However, research by Chaallal and Shahawy (2000) on rectangular RC beam-columns wrapped with bi-directional CFRP has shown

that the jacket can also confine the concrete on the compression side of members subjected to flexure, even when the opposite side of the member is in tension.

2.3. AXIALLY COMPRESSED FRP-CONFINED CONCRETE

2.3.1. General Behavior. In the course of attempting to understand the behavior of a new type of structural element, much attention must be given to fundamentals. For this reason, a great deal of work has been done researching the behavior of small axially loaded specimens of plain concrete confined by FRP. Such studies become the basis on which more complex applications may be founded. However, since many investigators have carried out very similar projects, there are some results that one finds frequently repeated. With this in mind, a short discussion of the commonly reported properties of FRP-confined concrete and the definition of some terms will be given before the unique results of individual researchers are presented.

As shown in Figure 2.2 by the upper two curves, the axial stress-axial strain curves of concrete passively confined by FRP are essentially in two parts with a small transition zone at the point of slope change. For the sake of discussion, the initial portion of the curve will be referred to as the elastic zone and the portion to the right of the transition zone as the plastic zone.

The slope of the elastic portion of the curve is essentially identical to that of the unconfined concrete. The type of jacket with which the concrete is confined has little effect on this portion of the curve, except that a stiffer jacket tends to mildly increase the stress and strain at which the transition zone occurs. The stress-strain curve of unconfined concrete is plotted with the confined concrete curves for comparison (see Figure 2.2). The reason the confined and unconfined curves are very similar in the elastic zone is that concrete undergoes little lateral expansion under small loads and thus does not react against the restraint of the jacket to produce confinement pressure.

The plastic zone occurs shortly after the peak strength of the unconfined concrete has been reached. At this point, the concrete is expanding rapidly because of its plastic

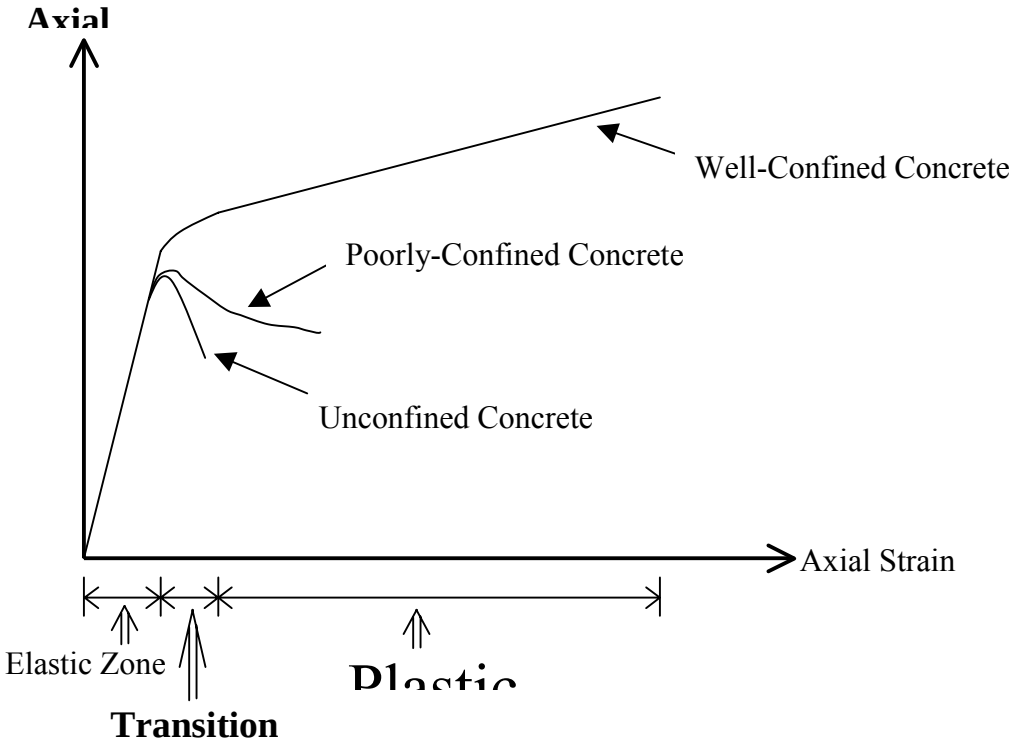

Figure 2.2. Typical Shape of an Axial Stress-Axial Strain Curve for Concrete Passively Confined by FRP

behavior and has fully activated the jacket. In the plastic zone, a small increase in stress causes a large (relative to the elastic zone) increase in radial expansion. This expansion causes two actions: first, it deteriorates the condition of the internal structure of the concrete. Second, it causes increased confining pressure; since, as may be recalled from Section 1, the fibers in the jacket exhibit linear elastic behavior until failure. These two actions help define the slope of the plastic portion of the curve. If the concrete is well-confined, then the slope will be positive and usually quite linear, indicating that the confining pressure is sufficient to curb the effect of the deteriorating condition of the concrete and allow greater stress to be applied. If the concrete is not well-confined, then the peak axial stress will be similar to that of unconfined concrete, indicating that the confining pressure is not sufficient to overcome the effect of the degradation of the

concrete under the large strains it is experiencing. A stiffer jacket tends to make the slope of the plastic zone more positive.

Finally, many investigators monitor the strain in the fibers in the FRP jackets as their specimens are loaded. Often they report that the ultimate tensile strain achieved by the fibers in the jackets before rupture is significantly less than the ultimate fiber strain achieved during coupon tests. This result is to be expected for three primary reasons. First, flat coupons are usually not as difficult to fabricate as jackets and therefore may be of higher quality. Second, the fibers in a coupon test are subject only to axial loads. In contrast, expanding concrete causes both axial loading and loading transverse to the axis of the fibers in a jacket. Lastly, the confined concrete may cause areas of localized fiber distress (stress concentrations) as it shifts and crushes beneath the jacket (Xiao and Wu 2000).

2.3.2. Various Research Findings. Steel has been used for many years to confine concrete, and the behavior of steel-confined concrete has been studied extensively. Why not simply use the models developed for steel-confined concrete on FRP-confined concrete? As it turns out, the equations that have been successfully used to model steel-confined concrete have been shown to be inaccurate when applied without modification to FRP-confined concrete. Hence, there arises a need for additional research and modeling. Saafi et al. (1999) give some explanation for why steel-confined concrete behaves differently than FRP-confined concrete. The difference, of course, lies in the differences in the material properties between FRP and steel. More specifically, however, the fibers in FRP behave elastically until rupture, while steel begins to behave inelastically long before it ruptures. Also, under adequate confinement, FRP-confined concrete attains its maximum axial stress and strain simultaneously (see upper curve in Figure 2.2). Steel-confined concrete, on the other hand, begins to lose strength after the steel yields.

Toutanji (1999) undertook to test eighteen cylindrical specimens 76 mm in diameter and 305 mm in length. Twelve of the specimens were jacketed with FRP while the

remaining six were unjacketed. Three types of FRP sheets were used to construct the jackets: glass, one type of carbon having a high tensile strength and another type of carbon having a high elastic modulus. Three groups of jacketed specimens were prepared, each group being jacketed with a different type of fiber. To jacket the specimens, two layers of the appropriate type of fiber were applied at 90 degrees in continuous laps. An epoxy resin system was used to bond the sheets to the cylinders. To ensure parallel ends, the specimens were sulfur capped. Strain gages applied at middle height on the surface of the jackets measured the axial and lateral strains.

The gain in ultimate compressive strength of the jacketed cylinders over the unjacketed cylinders was about 100% for the glass fibers and 200% for both types of carbon. The failure mode of the jacketed cylinders was observed to be rupture of the FRP sheets with little warning of impending failure, especially for the high modulus carbon fibers.

A model was proposed to predict the axial stress-axial strain curves of the confined concrete. It was developed as two intersecting curves to accurately depict the shape of the two-part experimental curves, which were similar in shape to the upper curve in Figure 2.2. The intersection of the two curves, which corresponds to the transition zone, was chosen to be the point where the lateral strain (the strain in the hoop direction in the jacket) reached 0.002. This value satisfied experimental observations. It was also consistent with the equations used to develop the model, which were based on equations originally postulated for concrete confined with steel. Since steel is normally elastic up to a strain of about 0.002, it seems reasonable that steel-confined concrete and FRP-confined concrete would behave similarly below this level of lateral strain.

The model, which is valid only for circular cross sections, was compared against the experimental results of other studies and found to compare favorably with most of them. Of particular note, is that provision was made in the model to handle cylinders confined with continuous jackets as well as cylinders confined with FRP tapes helically wound

around the cylinders at a given pitch. The model was shown to overestimate the ultimate compressive strength of concrete confined by unbonded FRP tubes.

Saafi et al. (1999) suggested that perhaps the difference between the model and the experimental data from concrete-filled FRP tubes results from the fact that the jackets for which the model was derived were strongly bonded to the concrete, while the tubes were not. It is certainly possible that this is the case. However, an earlier paper by Mirmiran et al. (1998), as discussed later in this section, indicates that for circular cross sections, adhesive bonding between the FRP and concrete makes little difference in the behavior of the specimen.

Perhaps the question of why the model did not accurately account for the confining effect of concrete confined by FRP tubes prompted Toutanji to join Saafi and Li (Saafi et al. 1999) in another research project focusing on FRP tubes. Their experimental program consisted of thirty cylindrical specimens, eighteen of which were concrete-filled FRP tubes and twelve of which were plain concrete. The size of the specimens was chosen to model short columns, their length and diameter being 435 mm and 152.4 mm, respectively, giving them a length-to-diameter (l/d) ratio of 2.85. Two types of fibers were used to construct the tubes, glass and carbon. The fibers in the tubes were oriented at 90 degrees. Three different thicknesses of tubes were constructed for each of the two fiber types. To avoid direct axial loading of the tubes, load from the testing machine was applied to the concrete core of the specimens through the use of circular pads. Two LVDT's measured axial strain by detecting the movement of steel platens used to transfer load from the machine to the cylinders. Surface strain gages bonded to the surface of the tubes measured both hoop and longitudinal strain.

As expected, the concrete-filled FRP tubes performed better than the unconfined specimens with regard to both strength and ductility. In general, an increase in the thickness of the tube resulted in both an increase in the ultimate strain and strength of the cylinders and an increase in the slope of the plastic part of the curve. The specimens with

tubes made of glass were observed to have significantly higher axial strains than the specimens with carbon tubes.

The researchers point to the fact that carbon fibers have a lower ultimate strain than glass fibers to explain why the glass tubes caused the greatest axial strain. This is logical, since for a given volume of concrete, the greater the dilation of the cross section due to the stretching of the tube, the greater the axial shortening required to maintain that volume. However, the dilation of the cross section is probably not the only contributor to axial deformation. As mentioned later in this section, other investigators have found that the volume of the concrete changes slightly during loading and may actually decrease with sufficient confinement. A decrease in volume of the specimen would allow for axial strain without corresponding dilation of the cross section.

Failure was marked by fracture of the tubes, the carbon tubes tending to fail more suddenly and violently than the glass tubes. Some local buckling in the tubes was observed prior to failure, which indicates that the tube was experiencing some axial load despite the use of the pads mentioned above. However, it was also observed that the failed tubes did not have concrete attached to their inner faces, revealing an absence of bonding at the interface of the materials.

The researchers proposed a model to predict the entire axial stress-axial strain curve of FRP-tube-confined concrete. It was derived in much the same way as Toutanji's model of FRP-jacketed concrete (Toutanji 1999). Again, the curve was composed of two straight lines whose intersection occurred when the hoop strain in the jacket reached 0.002. The experimental values were compared with the current model as well as with other models from the literature. The experimental data was shown to agree most closely with the proposed model.

Mirmiran and Shahawy (1997) tested twenty-four concrete-filled FRP tubes and six unconfined concrete specimens. All specimens were cylindrical, having 305 mm lengths and 152 mm diameters. Cement type II was used to minimize shrinkage, as it was

anticipated that shrinkage might delay the confinement effect of the tube. The results of the experiment indicated, however, that shrinkage is not likely to significantly effect the behavior of tube-confined concrete. The tubes were composed of a polyester resin and glass fibers in a ±75-degree configuration. After casting the specimens, grooves were cut in the tubes through their entire thickness at 19 mm from the ends around the entire circumference to prevent direct axial loading of the tubes. All specimens were sulfur capped. Lateral stains were measured by strain gages on the surfaces of the tubes. Longitudinal strains were measured by LVDT's and, on some specimens, by embedded strain gages.

Failure of the tubes was sudden but somewhat predictable. Near the ultimate state of loading, the investigators heard the sound of inner glass fibers rupturing and saw white patches, a sign of distress in the resin, forming in the tubes. One specimen was subjected to three loading-unloading cycles to determine its stiffness degradation under repeated loading. The failure of this specimen was similar to the others, and it was noted that the width of the hysteresis loops were not as large as for steel-encased concrete.

In the course of analyzing the test data, plots were made of the dilation rate versus the axial strain, where the dilation rate was defined as the rate of change of the lateral strain with respect to the axial strain. These plots showed that the dilation rate first increases to some maximum peak value, then decreases and finally reaches a constant asymptotic value, which it maintains until specimen failure.

Mirmiran et al. (1998) studied three different parameters to ascertain their effect on concrete confined by FRP. The investigation included tests of the effect of cross-sectional shape, l/d ratio, and bond.

The testing matrix used to determine the effect of shape consisted of twelve concrete-filled FRP tubes with square cross sections (152.5 mm x 152 mm x 305 mm) and thirty specimens with circular cross sections (152.5 mm in diameter and 305 mm in length). The tubes were constructed of a polyester resin and glass fibers wound at ±75 degrees.

Three different tube thicknesses were used. Again the tubes were grooved 19 mm from each end to avoid direct loading of the tubes. All specimens were sulfur capped prior to testing. Surface strain gages were used to measure the hoop strain in the tube and LVDT's were used to measure the longitudinal strain. In addition, certain specimens were fitted with both embedded and surface strain gages oriented to measure the longitudinal strain.

As in the tests described above by Mirmiran and Shahawy (1997) the cylinders showed patches of white attributed to yielded resin near their midsection at 60-70% of the ultimate load. For the square tubes these patches occurred only along the edges. For the specimens with circular cross sections, failure occurred when fibers ruptured near the midsection of the specimen, after which the specimen took no additional load. For the square cross sections a popping noise produced by localized fiber rupture would precede a load drop and subsequent stabilization at a lower value. Tube rupture generally occurred along the edges of square specimens.

The axial stress-axial strain curves were quite different for the two cross sections. The circular cross sections produced curves similar to the upper curve in Figure 2.2, while the specimens with square cross sections were characterized by curves similar to the curve labeled "Poorly-Confined Concrete" in Figure 2.2. Also, while the thickness of the jacket made a marked difference in the ultimate strength of the cylinders, an increase in the thickness of the square tubes had minimal impact on the ultimate strength, though some changes in the post-peak ductility were observed. The researchers attributed the differences between the two cross sections to differences in the distribution of the confining pressure. In the cylinders the confining pressure is uniform and dependent on the ultimate hoop strength available in the jacket. With square cross sections the pressure is maximum at the corners and of lesser magnitude in between dependent on the flexural rigidity of the sides of the FRP tube.

The effect of l/d ratio was studied using twenty-four cylinders 145 mm in diameter. Tubes of three different thicknesses were used and were constructed as described for the

shape-effect tests. Four tube lengths of 305 mm, 457 mm, 610 mm, and 762 mm were used, corresponding to l/d ratios ranging from 2:1 to 5:1. These specimens were sufficiently stocky to be considered as short columns. Specimens were sulfur capped and grooved as before. Surface-mounted strain gages measured hoop strain and longitudinal strain. LVDT's were also employed to measure longitudinal deformation.

For the range of l/d ratios studied in this testing program, there was little difference in the response of the columns, except that the 2:1 ratio did tend to outperform the more slender specimens in both ultimate axial stress and strain.

Previous research has shown that bonded steel tubes experience more axial load than unbonded steel tubes, which tends to lessen their confinement effect. It was thus thought expedient to investigate the effect of bond on FRP-confined concrete. Both circular and square cross sections were studied.

For the circular cross sections, thirty-two cylindrical specimens (152.5 mm in diameter by 305 mm in length) with both adhesively bonded and unbonded jackets were constructed. The data acquisition instrumentation was the same as for the shape-effect specimens. Two different methods were used to fabricate the jackets. Some jackets were made by repeated revolutions of a single continuous sheet of fiber around the specimens, while others were made from individual sheets of fiber applied one at a time to form the jacket. For the latter method, overlapped regions were created in each layer as a result of applying sheets whose length was greater than the circumference of the cylinders. These overlapped regions allowed the strength of the fibers to be developed in each layer, so that no weak seams were created. The overlapped regions were offset as each layer in the tube was laid in place. Only the unbonded specimens were grooved at the top and bottom; since, due to the bond, axial loading of the bonded jackets could not be avoided.

The results of the test showed no significant differences for either the bond effect or for the method of jacket fabrication. Interestingly, some of the most heavily confined specimens had a capacity that exceeded that of the testing machine. The investigators

attempted to fail some of these specimens by subjecting them to three additional cycles of loading and unloading but were unsuccessful. They took this opportunity to examine the concrete core by cutting the jackets off both a bonded and an unbonded specimen. For the unbonded specimen, the jacket showed no signs of distress and easily separated from the concrete once having been cut along its length. The concrete core was intact but had a horizontal crack perpendicular to its longitudinal axis that caused the cylinder to split in half when dropped on the floor. In the bonded specimen, the cutting of the jacket caused a release of stresses in the jacket, which resulted in circumferential cracks forming around the perimeter of the concrete core.

Concrete-filled FRP tubes were used to test the effect of bond on the square cross sections. A mechanical rather than adhesive bond was provided by including ribs made of polyester paste and chopped glass fibers on the inside faces of the tubes. The outer dimensions of the tubes were 178 mm x 178 mm x 305 mm. Three specimens were tested. Again, since the specimens were bonded, they were not grooved. However, the ends of the specimens were ground and capped with 5-mm thick lead plate. The lead covered the entire cross section for two of the specimens and only the concrete core for the third. This third specimen was found to fail at a slightly higher load than the ones with the load applied to both the core and the jacket.

The ribbed specimens exhibited greatly improved ultimate strength and strain over similar previously tested unbonded concrete-filled FRP tubes. Given these results, it appears that bond makes a large difference for concrete-filled FRP tubes with square cross sections, but bond makes little difference for those tubes with circular cross sections. Drawing such a conclusion assumes, however, that the other variables between the circular and square cross sections did not significantly influence the test results. For example, the addition of ribs to the square tubes may have caused some increase in performance not directly related to bond, but rather to the increased flexural rigidity of the sides of the tube.

Picher et al. (1996) performed tests on a series of twenty-seven cylinders and short concrete columns encased in three, four or five-ply jackets made of CFRP sheets. Fifteen cylinders (152 mm in diameter and 304 mm in length) were included in the testing program, as well as eight specimens with square cross sections (152 mm x 152 mm x 500 mm) and four with rectangular (152 mm x 203 mm x 500 mm) cross sections. Varying corner radii were given to the non-circular sections (5 mm, 25 mm, and 38 mm). Fiber orientations other than 90 degrees were given to some of the circular sections and to one of the square sections. All specimens were loaded under strain control at a rate of 10 με/s.

The motivation behind giving varying fiber orientations to some of the jackets was the hope that the failure mode of the jackets could be improved. No improvement was noted, however. In fact, one of the square specimens with a five-ply jacket, having four plies oriented at 75 degrees and one ply at 90 degrees, sustained less axial stress and axial strain than a similar specimen with four plies oriented at 90 degrees.

For specimens having non-circular cross sections, failure of the composite jackets occurred at or near the corners. The researchers attributed this behavior to stress concentrations. Increasing the corner radii caused increased ultimate axial stress and strain, which was described as a result of two actions: first, with increased corner radii, stress concentrations at the corners are not as severe. Second, the larger radii cause the specimen to become more circular.

For the square and rectangular cross sections, the radial strain was measured by LVDT's oriented perpendicularly to the sides of the specimens and placed in the center of the specimen between the corners. These LVDT's essentially measured the bulge in the jacket during testing. The radial strain in the square and rectangular specimens was consistently two to three times the axial strain. This result is in contrast to the cylinders, whose ultimate radial strain was usually lower than the ultimate axial strain. The greater radial strain in the non-circular sections is not surprising, given the location at which it was measured and given that the flexural strength of the jacket (the portion spanning

between the corners) is not large. The investigators noted that as the sides of a non-circular column bulge outward, then the cross section becomes more circular and thus more effective at confining the concrete. However, this increase in confinement effectiveness comes at the cost of much lateral expansion, which is detrimental to the internal structure of the concrete core.

Xiao and Wu (2000) performed tests on standard cylinders wrapped with one, two, and three-layer jackets of carbon sheets. The fiber orientation was 90 degrees. Lower, middle and high strength concrete specimens were constructed whose unconfined concrete strengths were slightly higher than 27.6 MPa, 37.9 MPa and 48.3 MPa, respectively. The cylinders were sulfur capped before testing. Axial deformation data were acquired using a specially fabricated device that measured the deformation of the specimens over a gage length of 152.4 mm in the middle of the cylinder. The researchers chose this position to measure axial deformation in order to avoid incorporating the effect of confinement from platen friction at the ends of the specimens. Longitudinal and transverse strains were measured in the jacket using stain gages. Coupon tests showed that the ultimate tensile strain in the fibers in the jackets was only about 50% to 80% of the ultimate strain recorded for the coupons.

Failure of the specimens resulted from fiber rupture. The experimental axial stress-axial strain curves were similar to the upper curve in Figure 2.2.

The investigators noted that after a certain amount of loading, the relationship between axial strain and lateral strain stabilizes to a linear relationship whose slope depends on the concrete strength and the jacket stiffness. This is exactly what Mirmiran and Shahawy (1997) observed using unbonded FRP tubes, reporting that the dilation rate (rate of change in lateral strain with respect to axial strain) of the concrete stabilized to an asymptotic value that depended on the concrete strength and jacket stiffness. In other words, saying that the dilation rate versus axial strain is constant is equivalent to saying that the axial strain versus lateral strain is linear.

A model was proposed that consists of two straight intersecting lines. The first line is based on elastic theory, which combines the effect of Poisson's ratio of the concrete and the elastic modulus of both the concrete and the carbon jacket. This line extends until it intersects with the second line at a stress equivalent to the unconfined concrete strength. This first line captures the behavior of the initial part of the elastic portion of the experimental curve, but it tends to overestimate the stiffness of the experimental curve as it approaches the transition zone. Equation 2.1 gives the form of the second line in the model.

$$f_{cz} = \alpha f'_c + k f_r \qquad \text{Equation 2.1}$$

In the above equation, f_{cz} is the stress in the concrete, f'_c is the strength of the unconfined concrete and f_r is the confining pressure. The parameters α and k are determined experimentally.

One interesting result of this experiment is that the data suggest that when the ratio of the modulus of the jacket to the square of the strength of the unconfined concrete is less than 0.2, then the plastic portion of the experimental axial stress-axial strain curve will be descending. Likewise, when it is greater than 0.2, then the plastic portion will be ascending.

Nanni and Bradford (1995) tested three groups of sulfur-capped cylindrical specimens (300 mm long and 150 mm in diameter). LVDT's were used to measure the movement of the crosshead of the testing machine in order to determine longitudinal strain. In a paper describing the research, a letter designated each group of specimens. This convention will be adopted for the following summary.

Group A consisted of sixteen cylinders helically wrapped with three sizes of AFRP tape pretensioned to 4 MPa and wound at pitches of 0 mm, 25 mm and 50 mm. The pretensioning ensured that no undue dilation of the concrete core was necessary to tighten the tape to begin its confining action. Group E consisted of fifteen cylinders filament

wound with epoxy-impregnated glass fibers at an 88-degree orientation. No pretensioning was used due to the risk of breaking individual fibers during winding. Prior to jacketing, the cylinders for the bonded specimens were coated with an epoxy primer, while unbonded ones were coated with a paste wax. Four thicknesses of jackets were used. Group F consisted of glass-aramid preformed FRP shells.

In Group A, all specimens with AFRP tape at a pitch of 50 mm had a cone-type failure followed by tape rupture with only a small strength improvement. The axial stress-axial strain of these specimens showed a plateaued region, which corresponded to where the concrete spalled between the spiraled tape. Significantly more confinement was achieved in the other specimens, which led the researchers to conclude that between 25 mm and 50 mm was the maximum pitch for which one could expect to achieve confinement of a cylinder along its entire length.

For Group E, the axial stress-axial strain curves were typical of FRP-confined cylinders. The ultimate axial strength and strain in the unbonded specimens were only slightly lower than for the bonded specimens.

The specimens in Group F experienced premature failure along longitudinal joints in the jackets created as a result of the method of fabrication.

Karbhari and Gao (1997) developed two models to predict the ultimate axial stress and strain in circular composite-confined concrete members. One model was empirically derived. The other model was more analytical, a decided attempt at modeling the ultimate behavior based on material properties, and not on any particular set of data obtained from FRP-confined concrete tests. The ultimate strength predictions for both models were based on equations similar in form to Equation 2.1. The model that empirically predicts ultimate strain was based on the assumption that ultimate strain is directly dependent on the ultimate strength of the FRP. The other model predicted ultimate strain from material properties through the assumption that the volume of the jacketed cylinder at ultimate is the same as that of the cylinder in the transition-zone state

of loading. This assumption appears reasonable, given that Mirmiran and Shahawy (1997) reported a total volume change of less than 2% for their FRP-confined specimens.

The proposed equations and three other sets of equations developed by other investigators were then compared to three sets of experimental data. Somewhat unsatisfactory agreement is noted for all models, except in the case of the proposed empirical model, which displays good agreement with the data from which it was derived.

Harmon et al. (1998) tested a series of small concrete cylinders (102 mm long and 51 mm in diameter) confined in filament wound tubes made of glass fibers, as well as tubes made of carbon fibers. In all specimens the fiber orientation was 90 degrees. Axial and radial strains were measured using extensometers.

The results of the tests showed an approximate linear increase in the ultimate axial stress with an increase in fiber volume in the jacket. In addition, the ultimate radial strain was independent of the fiber volume, while the ultimate axial strain increased with increasing fiber volume.

For unconfined concrete cylinders under axial loading, volumetric strain is negative until the axial stress reaches about 85% of the unconfined strength of the concrete. After this level of stress, the volumetric strain increases rapidly as a result of cracking within the cylinder. In this study, high levels of confinement were observed to lead to negative ultimate volumetric strains. That is, large confining pressures actually caused the volume of the cylinders to decrease with increasing axial stress. Similar results were reported by Mirmiran and Shahawy (1997).

When analyzing the data, the researchers constructed plots of experimental axial stress versus analytically computed confinement stress for various types of jackets. The plots showed that as the jacket stiffness increases, a smaller confinement stress is needed to enable the cylinder to sustain a given axial load. This makes sense intuitively, given that

a stiffer jacket requires less radial expansion (and therefore less damage to the internal structure of the concrete) to induce a particular confinement pressure.

A new model to predict the behavior of FRP-confined concrete was proposed based on the concept of quantifying the internal friction in the concrete and relating it to stress and strain. The model assumes that total concrete strain is the sum of elastic strain, crack strain and void strain. These three types of strain are defined as follows:

- Elastic strain - linearly related to stress and recoverable upon unloading of the specimen
- Crack strain - occurs as a result of both slip between the two surfaces forming the crack and as a result of separation caused by the roughness of these surfaces as they slip past one another. The former causes axial compression and radial expansion, while the latter causes both radial and axial expansion.
- Void strain - occurs as a result of the collapse of voids within the concrete as stresses increase.

The model assumes that sliding of concrete along the crack path occurs when a critical combination of shearing and normal forces act on the crack surface as a result of confining pressures and axial load. Through a number of analytic expressions, empirical relationships and approximations based on experimental observations, the shear and normal stresses on the individual cracking planes are related to the global axial and radial stresses in the cylinder. At the same time, the crack slipping and separation are related to the global axial and global radial strains. These relationships lead to an iterative method of defining the axial stress versus axial, radial, and volumetric strain curves. In constructing their model, the authors accounted for only strain associated with elastic deformation and slipping along crack planes, making no attempt to account for void collapse. Some method to account for void collapse seems appropriate however, since their model was shown to tend to underestimate axial strain, and because their research indicated negative volumetric strain (compaction) in the confined concrete.

On a practical note, the model requires values for parameters that are characteristic of a given concrete mix and obtainable only through laboratory testing. Obtaining these parameters would make the implementation of this model difficult for design professionals, unless a database of parameters for various concrete mixes could be established.

The purpose of research performed by Liu et al. (2000) was to investigate the performance of unbonded, filament-wound, hybrid composite jackets on plain concrete cylinders. The specimens measured 100 mm in diameter by 200 mm in length. E-glass, Kevlar (a para-aramid fiber), and carbon fibers were filament wound around the cylinders under 15 N of tension. The cylinders were wound with six layers of fibers at various combinations of 45, 60 and 90-degree winding angles. The seven different combinations are as follows: $[90]_6$, $[\pm 60]_3$, $[\pm 45]_3$, $[\pm 45/90_2/\pm 45]$, $[\pm 60/90_2/\pm 60]$, $[90_2/\pm 45/90_2]$, $[90_2/\pm 60/90_2]$, where the numbers within each bracket represent the winding angle with respect to the longitudinal axis of the cylinder and the subscripts represent the number of layers of fiber. The "±" symbol represents two interlaced layers of fiber, one layer at a positive angle and the other at a negative angle. Also, for those brackets with multiple numbers, the sequence of the numbers describes the sequence of layering within the composite jacket. Thus, $[90_2/\pm 60/90_2]$ describes jackets composed of two 90 degree layers, followed by two layers interlaced at +60 and –60 degrees, and completed by another two 90 degree layers. Before filament winding, the specimens were wrapped with aluminum foil to ensure an unbonded condition. Three groups of filament wound specimens were tested. The first group consisted of cylinders wound only with glass fibers (G specimens) and included specimens with all of the seven winding-angle combinations mentioned above. The second group consisted of cylinders having two layers of carbon fiber sandwiched between two layers of glass on either side (GCG specimens). Only the $[\pm 45/90_2/\pm 45]$, $[\pm 60/90_2/\pm 60]$, $[90_2/\pm 45/90_2]$, and $[90_2/\pm 60/90_2]$ winding angles were used. The third group was similar to the second, but the two layers of glass were replaced with two layers of Kevlar (GKG specimens). For all three of the groups, three specimens were tested for each winding angle.

For the G specimens, the $[90]_6$ jacket resulted in the highest ultimate cylinder strength. For the rest of the G specimens, the closer the winding angle of the fibers was to 90 degrees the greater the ultimate strength of the specimen was. Thus, the $[\pm 60]_3$ jackets outperformed the $[\pm 45]_3$ jackets. Likewise, $[90_2/\pm 60/90_2]$ jackets were more effective than the $[90_2/\pm 45/90_2]$ jackets. In addition, the specimens with the $[\pm 60/90_2/\pm 60]$ jackets and the $[90_2/\pm 45/90_2]$ jackets were found to have nearly the same strengths. These trends were also found within the GCG and GKG groups.

Comparison of the results between the three groups showed that for a given winding angle, the G specimens were the strongest, followed by the GKG specimens and the GCG specimens, respectively. The authors explained this result to be a consequence of the modulus of elasticity mismatch and the ultimate strain mismatch that occurs when two kinds of fiber are working in the same jacket. For example, glass has a high failure strain and a low modulus, making it incompatible with carbon, which has both a high failure strain and a high modulus. Thus, in the GCG specimens, delamination occurred between the glass and carbon layers as a result of the different fiber strains caused by the different moduli. Also, the carbon reached its maximum strain earlier than the glass, leading to rupture of the carbon fibers before the strength of the glass fibers was fully realized. Similar incompatibility occurred within the GKG specimens but to a lesser degree.

The ordering of the three groups with respect to the greatest ultimate axial strain ran opposite of the strength results. The GCG specimens demonstrated the greatest ultimate strains, followed by the GKG specimens and the G specimens, respectively.

2.4. SUMMARY

As can be observed from the above discussion, the majority of previous research efforts related to concrete under pure axial loading have focused on plain concrete confined with FRP. This project will build upon that knowledge base by extending the testing to axially loaded RC columns, as described in the next section.

3. EXPERIMENTAL PROGRAM

3.1. GENERAL

The main objective of this study was to investigate the effect of several experimental variables on the confinement effectiveness of FRP jackets on rectangular RC columns. However, for reference purposes, circular columns were also included in the testing matrix. The experimental variables investigated included the following: the cross-sectional aspect ratio (ratio of the length of the long side of the cross section to that of the short side) of the column, the amount and type of fibers constituting the FRP jacket, the sharpness of the column corners, and the amount of longitudinal and transverse steel reinforcement in the column. As will be described in more detail below, all test specimens were of the same length and cross sectional area, subjected to the same type of loading, and manufactured with concrete of approximately the same strength.

3.2. SPECIMEN CHARACTERISTICS

Tests have been performed on twenty-six fourth-scale RC columns having a concrete strength of approximately 21 MPa. Ready-mix concrete was used for the manufacture of the columns. River gravel 9.5 mm in diameter was used as the coarse aggregate. All columns had a cross section of about 320 cm^2. Four columns had circular cross sections, whereas the other twenty-two columns had rectangular cross sections with aspect ratios of 1.0, 1.5 or 2.0. During testing, all columns were subjected to axial compression gradually applied in a few load-reload cycles of increasing magnitude until failure.

3.3. SPECIMEN NAMING SYSTEM

3.3.1. General. The test specimens have been given descriptive names. Throughout the remainder of this report, these names will often be used in lieu of the specimen number when referring to a specific column. The specimen names, as shown in the second column of Table 3.1, are composed of groups of numbers and letters separated by hyphens. Each of these descriptive groups gives information about some aspect of the column in this order: (1) jacketing scheme, (2) cross-sectional shape, (3) transverse

Table 3.1. Specimen Characteristics

Column No.	Column Name	Fiber Amount	Jacket Type	Cross-sectional Dimensions (mm)	Corner*	Lateral Reinf. Spacing (mm)
1	Ref-Circ-Sp51mm-ρ1.8	No fiber	---	203 (diameter)	13 mm chamfer	51 (spiral)
2	Ref-Circ-Ti178mm-ρ1.6			203 (diameter)		178
3	Ref-Rect$^{1}/_{1}$-Ti44mm-ρ1.6			181 x 181		44
4	Ref-Rect$^{1}/_{1}$-Ti178mm-ρ1.6			181 x 181		178
5	Ref-Rect$^{3}/_{2}$-Ti178mm-ρ1.6			146 x 222		178
6	Ref-Rect$^{2}/_{1}$-Ti178mm-ρ1.6			127 x 254		178
7	Ref-Rect$^{2}/_{1}$-Ti127mm-ρ1.6			127 x 254		127
8	1CFRP-Circ-Sp51mm-ρ1.8	1 ply	CFRP	203 (diameter)	**	51 (spiral)
9	1CFRP-Circ-Ti178mm-ρ1.6			203 (diameter)		178
10	2CFRP-Rect$^{1}/_{1}$-Ti178mm-ρ1.6	2 plies		181 x 181		178
11	2CFRP-Rect$^{3}/_{2}$-Ti178mm-ρ1.6			146 x 222		178
12	2CFRP-Rect$^{2}/_{1}$-Ti178mm-ρ1.6			127 x 254		178
13	2CFRP-Rect$^{2}/_{1}$-Ti127mm-ρ1.6	2 plies	CFRP	127 x 254	**	127
14	2CFRP-Rect$^{1}/_{1}$-Ti44mm-ρ1.6			181 x 181		44
15	2CFRP-Rect$^{1}/_{1}$-Ti102mm-ρ1.6					102
16	2CFRP-Rect$^{1}/_{1}$-Ti178mm-ρ0.9	2 plies	CFRP	181 x 181	**	178
17	2CFRP-Rect$^{1}/_{1}$-Ti178mm-ρ3.5					
18	2CFRP-Rect$^{1}/_{1}$-Ti178mm-ρ1.6-6.4mm	2 plies	CFRP	181 x 181	***	178
19	2CFRP-Rect$^{1}/_{1}$-Ti178mm-ρ1.6-19mm				****	
20	1CFRP-Rect$^{1}/_{1}$-Ti178mm-ρ1.6	1 ply	CFRP	181 x 181	**	178
21	1GFRP-Rect$^{1}/_{1}$-Ti178mm-ρ1.6	1 ply	GFRP	181 x 181	**	178
22	2GFRP-Rect$^{1}/_{1}$-Ti178mm-ρ1.6	2 plies				
23	3GFRP-Rect$^{1}/_{1}$-Ti178mm-ρ1.6	3 plies				
24	1AFRP-Rect$^{1}/_{1}$-Ti178mm-ρ1.6	1 ply	AFRP	181 x 181	**	178
25	2AFRP-Rect$^{1}/_{1}$-Ti178mm-ρ1.6	2 plies				
26	3AFRP-Rect$^{1}/_{1}$-Ti178mm-ρ1.6	3 plies				

* See Figure 3.3 and accompanying discussion in Section 3.7

** 13 mm chamfer rounded with 9.5 mm offsets

*** 6.4 mm chamfer rounded with 4.8 mm offsets

**** 19 mm chamfer rounded with 14 mm offsets

reinforcement arrangement, (4) percentage of longitudinal reinforcement and (5) corner sharpness. Each of these groups is described in detail below.

3.3.2. Jacketing Scheme. The first group describes the jacket. Ref, CFRP, GFRP and AFRP denote reference (unjacketed), carbon FRP, glass FRP and aramid FRP, respectively. The number preceding the jacketed columns refers to the number of sheets of FRP making up the jacket.

3.3.3. Cross-Sectional Shape. The second group describes the shape of the column cross section. Circ and Rect refer to circular and rectangular, respectively. The fraction proceeding the columns labeled with Rect refers to the aspect ratio of the column cross section.

3.3.4. Transverse Reinforcement Arrangement. The third group refers to the lateral reinforcement. Sp denotes a spiral column, while Ti denotes a tied column. The numbers proceeding the Sp and Ti designation refer to the center-to-center spacing of the reinforcement.

3.3.5. Percentage of Longitudinal Reinforcement. The fourth group describes the quantity of longitudinal reinforcement. The reinforcement ratio, ρ, is given in percent. It was computed by dividing the area of steel in the cross section by 320 cm^2, the approximate gross area of the column cross section.

3.3.6. Corner Sharpness. The 6.4mm and the 19mm designations comprising the fifth group refer to the size of the chamfer on the column corners. The fifth group is shown only on columns number 18 and 19, the specimens for which this parameter is a variable. For the remainder of the columns, the size of the chamfer is understood to be 13 mm. Smaller chamfers correspond to sharper corners. See Section 3.7 for more information on how the corners were rounded.

3.4. GROUPING THE SPECIMENS FOR COMPARISON

Table 3.2 shows the particular columns from Table 3.1 that will be compared against one another in the analysis of the experimental data. Each section of Table 3.2 represents a series of columns from which the effect of a particular test variable will be investigated.

3.5. DIMENSIONS OF SPECIMENS

Each specimen had a middle test region 914 mm long and two enlarged block-like ends with dimensions of 610 mm x 610 mm x 305 mm, as shown in Figure 3.1. This configuration forced general failure to occur in the test region and prevented premature failure at the ends. The enlarged ends also served to stabilize the column during testing and to simulate the general column-foundation or column-slab/beam interface. The test region of 914 mm was about 3.5 to 5 times greater than the larger dimension of the cross section to allow for a uniform strain and stress distribution in this region.

3.6. REINFORCEMENT ARRANGEMENT

The rectangular columns were reinforced with four longitudinal rebars, one located at each corner of the cross section. In the case of the circular columns, the longitudinal rebars were arranged uniformly about the perimeter of the cross section. The tied circular columns were reinforced with four longitudinal bars, while the spiral columns were reinforced with eight. In the test region of the specimens, 13 mm of clear cover was provided for the transverse reinforcement in the non-circular columns, while circular tied columns and spiral columns were provided with 21 mm and 16 mm of clear cover, respectively. Transverse reinforcement consisted of 6.35-mm smooth dowel. Columns number 1, 3, 8, and 14 (see Table 3.1) were reinforced with continuous spiral reinforcement or closely spaced ties to provide the necessary confinement according to ACI 318-95 requirements for seismic design. Circular ties were fabricated with 51-mm extensions on 90-degree hooks, while the non-circular ties were fabricated with 76-mm extensions on 135-degree hooks. Figure 3.2 shows reinforcement details.

Table 3.2. Specimen Groups and Corresponding Investigated Variables

Column No.*	Column Name**	Variable Under Investigation
16	2CFRP-Rect$^{1}/_{1}$-Ti178mm-ρ0.9	Amount of Longitudinal Reinforcement
10	2CFRP-Rect$^{1}/_{1}$-Ti178mm-ρ1.6	
17	2CFRP-Rect$^{1}/_{1}$-Ti178mm-ρ3.5	
4	Ref-Rect$^{1}/_{1}$-Ti178mm-ρ1.6	Corner Sharpness
18	2CFRP-Rect$^{1}/_{1}$-Ti178mm-ρ1.6-6.4mm	
10	2CFRP-Rect$^{1}/_{1}$-Ti178mm-ρ1.6	
19	2CFRP-Rect$^{1}/_{1}$-Ti178mm-ρ1.6-19mm	
1	Ref-Circ-Sp51mm-ρ1.8	Tie Spacing for Circular Cross Sections
2	Ref-Circ-Ti178mm-ρ1.6	
8	1CFRP-Circ-Sp51mm-ρ1.8	
9	1CFRP-Circ-Ti178mm-ρ1.6	
20	1CFRP-Rect$^{1}/_{1}$-Ti178mm-ρ1.6	Circular vs. Square Cross Section
9	1CFRP-Circ-Ti178mm-ρ1.6	
6	Ref-Rect$^{2}/_{1}$-Ti178mm-ρ1.6	Tie Spacing for Cross-Sectional Aspect Ratio of 2.0
7	Ref-Rect$^{2}/_{1}$-Ti127mm-ρ1.6	
12	2CFRP-Rect$^{2}/_{1}$-Ti178mm-ρ1.6	
13	2CFRP-Rect$^{2}/_{1}$-Ti127mm-ρ1.6	
3	Ref-Rect$^{1}/_{1}$-Ti44mm-ρ1.6	Tie Spacing for Cross-Sectional Aspect Ratio of 1.0
4	Ref-Rect$^{1}/_{1}$-Ti178mm-ρ1.6	
14	2CFRP-Rect$^{1}/_{1}$-Ti44mm-ρ1.6	
15	2CFRP-Rect$^{1}/_{1}$-Ti102mm-ρ1.6	
10	2CFRP-Rect$^{1}/_{1}$-Ti178mm-ρ1.6	
10	2CFRP-Rect$^{1}/_{1}$-Ti178mm-ρ1.6	Aspect Ratio
11	2CFRP-Rect$^{3}/_{2}$-Ti178mm-ρ1.6	
12	2CFRP-Rect$^{2}/_{1}$-Ti178mm-ρ1.6	
5	Ref-Rect$^{3}/_{2}$-Ti178mm-ρ1.6	Wrapped vs. Unwrapped for Cross-Sectional Aspect Ratio of 1.5
11	2CFRP-Rect$^{3}/_{2}$-Ti178mm-ρ1.6	
4	Ref-Rect$^{1}/_{1}$-Ti178mm-ρ1.6	Thickness of CFRP Jacket
20	1CFRP-Rect$^{1}/_{1}$-Ti178mm-ρ1.6	
10	2CFRP-Rect$^{1}/_{1}$-Ti178mm-ρ1.6	
4	Ref-Rect$^{1}/_{1}$-Ti178mm-ρ1.6	Thickness of AFRP Jacket
24	1AFRP-Rect$^{1}/_{1}$-Ti178mm-ρ1.6	
25	2AFRP-Rect$^{1}/_{1}$-Ti178mm-ρ1.6	
26	3AFRP-Rect$^{1}/_{1}$-Ti178mm-ρ1.6	

Table 3.2. Specimen Groups and Corresponding Investigated Variables (Continued)

Column No.*	Column Name**	Variable Under Investigation
4	Ref-Rect$^{1}/_{1}$-Ti178mm-ρ1.6	Thickness of GFRP Jacket
21	1GFRP-Rect$^{1}/_{1}$-Ti178mm-ρ1.6	
22	2GFRP-Rect$^{1}/_{1}$-Ti178mm-ρ1.6	
23	3GFRP-Rect$^{1}/_{1}$-Ti178mm-ρ1.6	

* Represents the column number as listed in Table 3.1.
** For all jacketed columns not showing a corner chamfer, it is understood to be 13 mm.

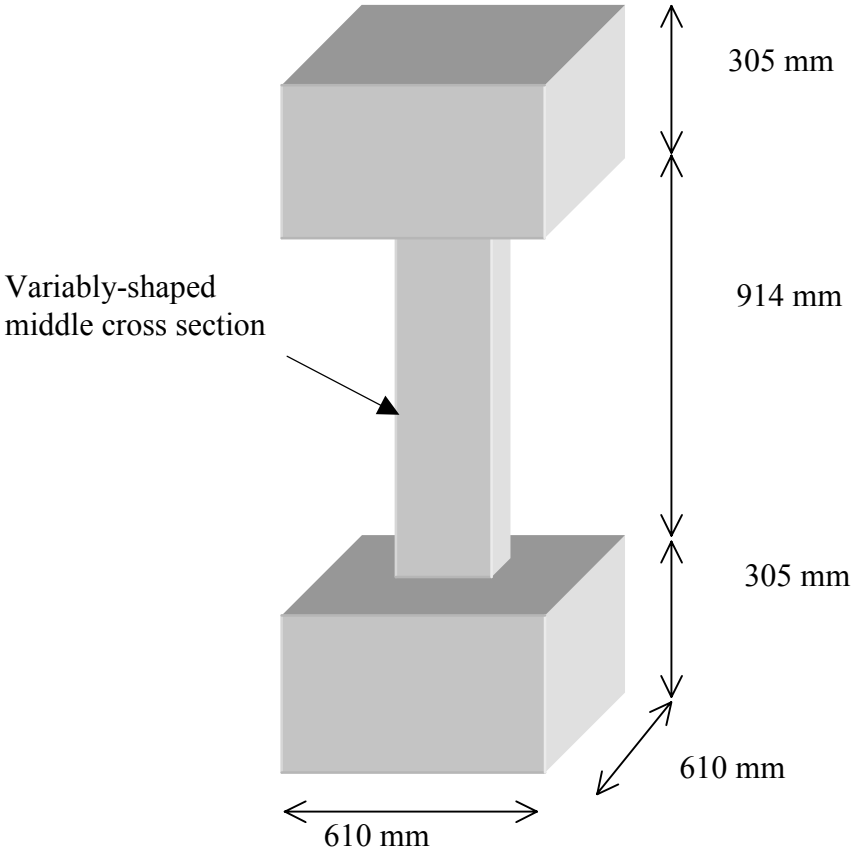

Figure 3.1. Column Dimensions

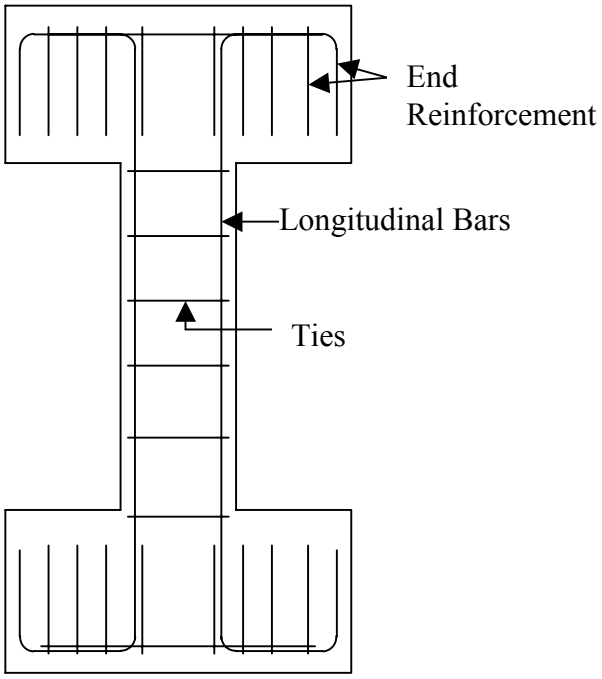

Figure 3.2. Schematic of Reinforcement Arrangement

3.7. CORNER ROUNDING

The corners of the rectangular and square columns are rounded with varying degrees of sharpness. The columns, having been chamfered during construction, were marked along their length with lines that were parallel to and offset from the edges of the chamfered corners. The columns were then ground, so that the finished corners were a semi-elliptical shape as shown by the dashed line in Figure 3.3. All of the non-circular cross sections received a 13-mm chamfer and a 9.5-mm offset, except for the two columns for which the corner radius was a test variable. One of these two columns received a 6.4-mm chamfer and a 4.8-mm offset, while the other received a 19-mm chamfer and a 14-mm offset. Corner rounding is a well-accepted procedure that is commonly used when retrofitting rectangular RC columns with FRP composites. The importance of the effect of the sharpness of the corners comes into play when one considers the tradeoff between the expense of grinding larger, smoother corners and the increase in jacket performance that comes from this activity.

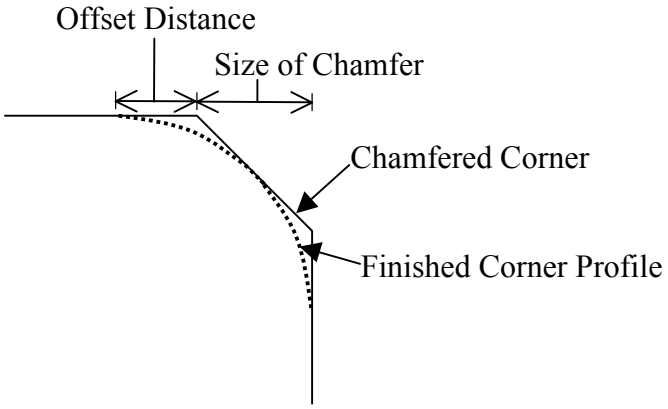

Figure 3.3. View of the Cross Section of a Non-circular Column at the Corner

3.8. JACKETING

Three types of fibers were used in this study, namely MBrace™ CF 130 High Tensile Carbon Fiber, MBrace™ EG 900 E-Glass Fiber and MBrace™ AK 60 Aramid Fiber. To jacket the columns, the concrete surface was first prepared by sandblasting. MBrace™ epoxy-based resins were then used in conjunction with the above-mentioned fibers to jacket the columns. First, a coat of primer was applied to ensure a good bond between the jacket and the column. Following the primer, a coat of putty was applied to fill surface flaws and produce a smooth surface. Finally, a saturant was used to saturate the fibers and bond them to the column. The fibers in the jackets were oriented at 90 degrees. The layers of fibers were applied one at a time, with each layer overlapping itself, as shown in Figure 3.4, to provide for development of the full tensile strength of the fiber sheet. The carbon sheets were overlapped 102 mm, while the aramid and glass sheets were overlapped 152 mm. No overlap was provided between adjacent sheets in the longitudinal direction (see Figure 3.5). The jacket thicknesses were varied by varying the number of sheets of fiber applied. For columns with multiple layers, the overlapped area of each layer of fiber was rotated 90 degrees from the overlapped area of the previous layer (see Figure 3.4). Seven columns (see Table 3.1) with different cross sections and reinforcement arrangements were tested without FRP strengthening to serve as benchmark tests.

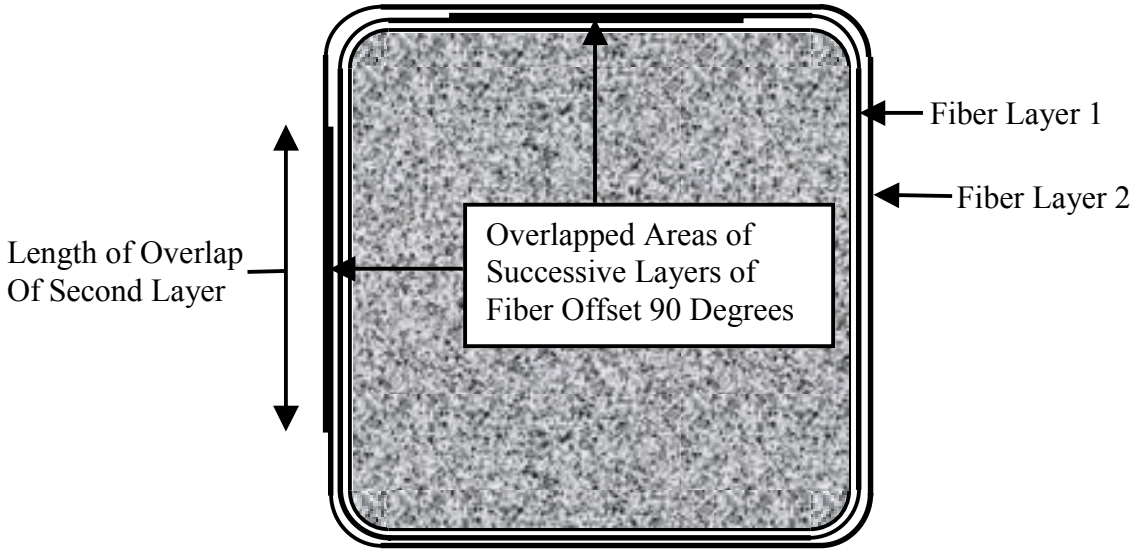

Figure 3.4. View of the Cross Section of a Jacketed Column

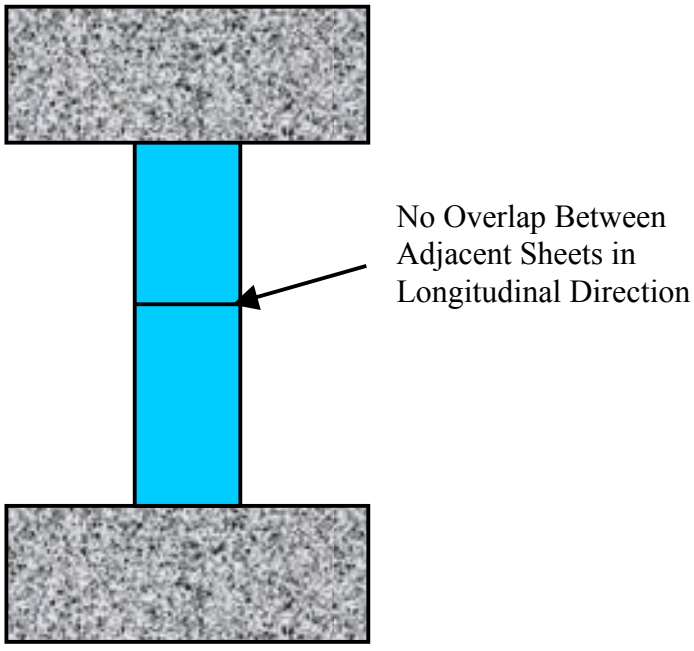

Figure 3.5. Elevation View of a Jacketed Column

3.9. LOADING AND INSTRUMENTATION

The axial load was applied using a 1780-kN Baldwin testing machine. The load was monitored using a 2220-kN load cell, located on top of the column as shown in Figure 3.6. Figure 3.7 shows a fully instrumented column ready for testing.

Figure 3.8 shows instrumentation details. Column lateral displacement was monitored at the center of the 914-mm test region using LVDT's, as illustrated in Figure 3.8a. In addition, the axial deformation of the specimen was measured using LVDT's as shown in Figure 3.8a and string transducers as shown in Figure 3.9. The LVDT's and string transducers had gage lengths of approximately 380 mm and 760 mm, respectively. For columns 4, 24, 25, and 26 (see Table 3.1), three LVDT's were used to measure longitudinal deformation. For the remaining columns one LVDT and two string transducers were used. The string for the string transducer was threaded through a pulley attached near the bottom of the test region and then tied near the top of the test region to an eyebolt screwed into the side of the column. The string transducer, having an internal spring-loaded recoil device, kept tension on the string and sensed the shortening of the string, which corresponded to the axial shortening of the column as it was loaded.

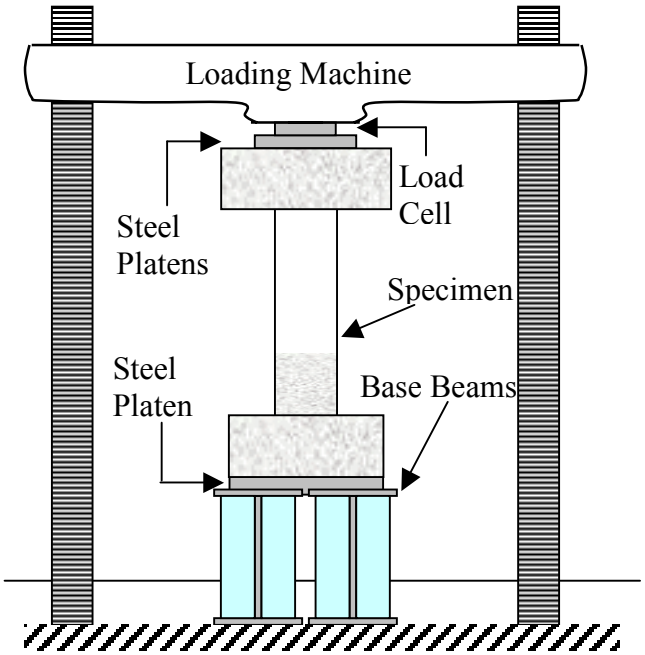

Figure 3.6. Schematic of Test Setup

Figure 3.7. Instrumented Column in Test Frame

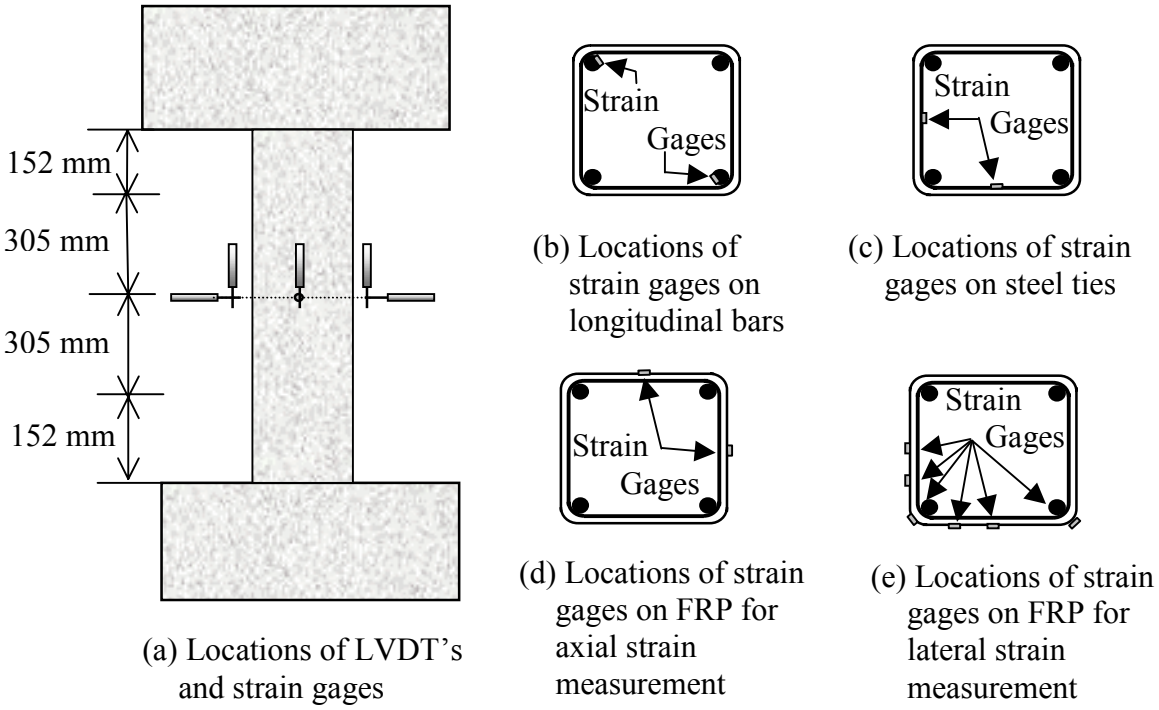

Figure 3.8. Instrumentation Details Showing Locations of LVDTs and Strain Gages

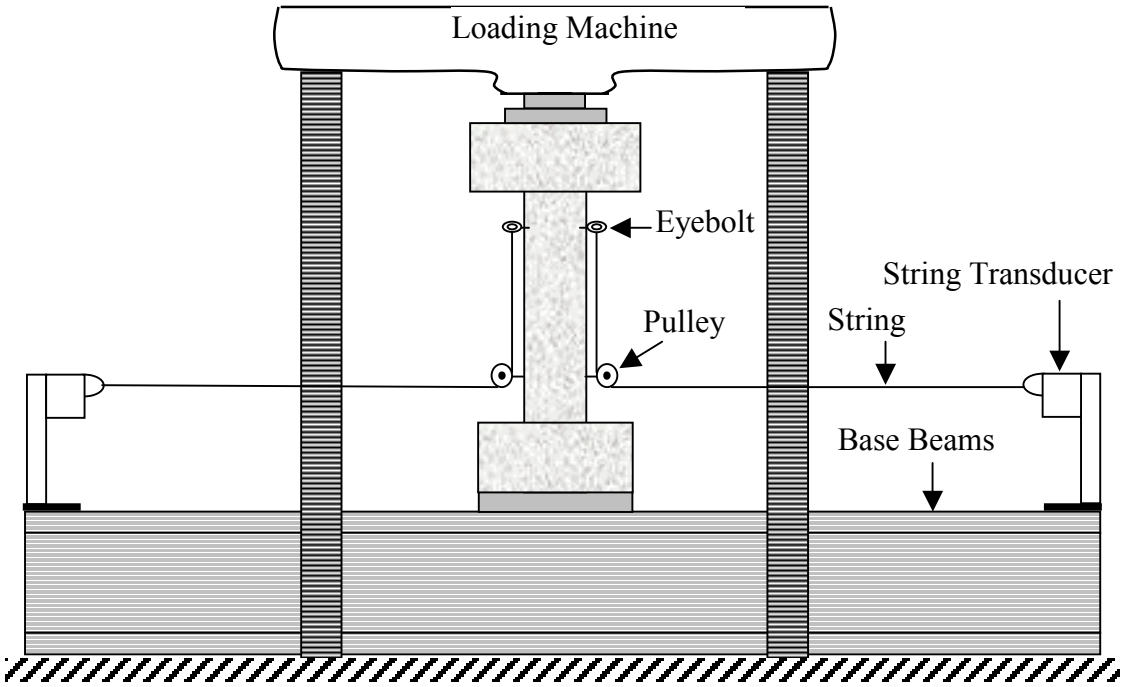

Figure 3.9. String Transducer Setup for Measuring Longitudinal Deformation

Strain gages monitored deformation in the steel reinforcing. Two strain gages were applied on the longitudinal reinforcement in the center of the testing region, one on each of two diagonally opposite steel bars, as pictured in Figure 3.8b. Four strain gages were applied on the lateral reinforcement, two on each of two ties as shown in Figure 3.8c. One of these ties was placed near the center of the test region and the other at approximately 150 mm from the end of the test region (the placement of the latter being dictated by the chosen lateral reinforcement spacing).

Axial strain on the FRP jacket was measured using strain gages having 51-mm gage lengths as shown in Figure 3.8d. Two of these strain gages were applied near the middle of the 914-mm testing region. For the non-circular cross sections, fiber strain in the hoop direction was measured using strain gages attached in the center of the 914-mm testing region at six points as shown in Figure 3.8e. For the circular cross sections, four strain gages were placed around the circumference of the column at 90-degree intervals. The strain gages were attached after the FRP jacket was applied and the resin had cured.

3.10. MATERIAL PROPERTIES

Table 3.3 summarizes the properties of the steel reinforcement used in the columns. The values shown in the table were obtained from monotonic tension tests.

Table 3.3. Properties of the Steel Reinforcing

Reinforcement Component	Surface Characteristics	Diameter (mm)	Yield Strength (MPa)
Longitudinal Bars*	Deformed	9.5	362
Longitudinal Bars**	Deformed	19.0	436
Longitudinal Bars***	Deformed	12.7	400
Spiral	Smooth	6.4	632
Ties	Smooth	6.4	427

* Used in columns number 1, 8 and 16
** Used in column number 17
*** Used in all columns except for the four columns listed in the first two notes above

Table 3.4 displays the properties of the fibers used to construct the FRP jackets. The data were provided by the manufacturer.

Table 3.4. Properties of the High Strength Fibers

Fiber Type	Guaranteed Ultimate Strength (MPa)	Load per Sheet Width (kN/m)	Tensile Modulus (GPa)	Guaranteed Ultimate Strain (%)
Carbon	3790	627	228	1.7
Aramid (Kevlar)	2000	559	117	1.7
E-Glass	1520	534	72.4	2.1

The columns were tested at varying ages, the youngest age being about two months and the oldest seven months. Because the columns were not all poured from the same batch of concrete, the axial loads sustained by the columns had to be normalized with respect to the strength of their companion cylinders. In most cases, these cylinders were allowed to cure in the same environment as their respective columns. The notable

exceptions were the columns indicated by an asterisk in Table 3.5, for which the cylinders remained outside for an interval of 3 to 4 weeks in winter weather conditions while the columns were inside the testing lab. The least mature concrete was about 28 days old when this separation occurred and 132 days old at testing.

Table 3.5 shows the age of the specimens when tested, as well as the age and strength of their corresponding cylinders. The cylinders were 152 mm in diameter by 305 mm in length. They were sulfur capped before testing and were loaded at a rate of 4.45 kN/s. The compressive strength shown in the fifth column of Table 3.5 represents the average strength of either 3 or 4 cylinders.

Table 3.5. Strengths and Ages of Specimens and Cylinders

Column No.	Column Name	Specimen Age at Testing (days)	Cylinder Age at Testing (days)	f'_c (MPa)
1*	Ref-Circ-Sp51mm-ρ1.8	203	223	19.6
2*	Ref-Circ-Ti178mm-ρ1.6	203	223	23.8
3	Ref-Rect$^{1}/_{1}$-Ti44mm-ρ1.6	111	128	19.8
4	Ref-Rect$^{1}/_{1}$-Ti178mm-ρ1.6	62	120	35.4
5	Ref-Rect$^{3}/_{2}$-Ti178mm-ρ1.6	111	128	19.8
6*	Ref-Rect$^{2}/_{1}$-Ti178mm-ρ1.6	133	150	24.5
7*	Ref-Rect$^{2}/_{1}$-Ti127mm-ρ1.6	133	150	24.5
8*	1CFRP-Circ-Sp51mm-ρ1.8	203	223	23.8
9*	1CFRP-Circ-Ti178mm-ρ1.6	204	223	23.8
10*	2CFRP-Rect$^{1}/_{1}$-Ti178mm-ρ1.6	188	207	26.3
11	2CFRP-Rect$^{3}/_{2}$-Ti178mm-ρ1.6	110	128	19.8
12*	2CFRP-Rect$^{2}/_{1}$-Ti178mm-ρ1.6	132	150	24.5
13*	2CFRP-Rect$^{2}/_{1}$-Ti127mm-ρ1.6	132	150	24.5
14*	2CFRP-Rect$^{1}/_{1}$-Ti44mm-ρ1.6	188	207	26.3
15*	2CFRP-Rect$^{1}/_{1}$-Ti102mm-ρ1.6	189	207	26.3
16	2CFRP-Rect$^{1}/_{1}$-Ti178mm-ρ0.9	208	230	25.2
17	2CFRP-Rect$^{1}/_{1}$-Ti178mm-ρ3.5	208	230	25.2
18	2CFRP-Rect$^{1}/_{1}$-Ti178mm-ρ1.6-6.4mm	208	230	25.2
19	2CFRP-Rect$^{1}/_{1}$-Ti178mm-ρ1.6-19mm	210	230	25.2
20	1CFRP-Rect$^{1}/_{1}$-Ti178mm-ρ1.6	185	233	19.6
21	1GFRP-Rect$^{1}/_{1}$-Ti178mm-ρ1.6	211	233	19.6

Table 3.5. Strengths and Ages of Specimens and Cylinders (Continued)

Column No.	Column Name	Specimen Age at Testing (days)	Cylinder Age at Testing (days)	f'c (MPa)
22	2GFRP-Rect$^{1}/_{1}$-Ti178mm-ρ1.6	210	233	19.6
23	3GFRP-Rect$^{1}/_{1}$-Ti178mm-ρ1.6	214	233	19.6
24	1AFRP-Rect$^{1}/_{1}$-Ti178mm-ρ1.6	65	120	35.4
25	2AFRP-Rect$^{1}/_{1}$-Ti178mm-ρ1.6	78	120	35.4
26	3AFRP-Rect$^{1}/_{1}$-Ti178mm-ρ1.6	88	120	35.4

* Specimen not cured with cylinders

3.11. SUMMARY

Twenty-six fourth-scale RC columns with variable cross-sectional geometries, steel reinforcement and FRP jacketing schemes have been tested in pure axial compression. The specimens were given descriptive names so that they may be discussed in Section 4 without frequent reference to Table 3.1. The specimens were instrumented with strain gages on both the steel reinforcing and the FRP jackets. In addition, the axial deformation of the columns was monitored with LVDT's and string transducers. The properties of the materials used to manufacture the test specimens have been summarized in Section 3.10.

4. TEST RESULTS

4.1. GENERAL

In this section the results of the testing program are presented. General observations concerning the failure of the columns, the effects of the various test variables and the behavior of the FRP jacket are discussed.

4.2. OBSERVATIONS OF SPECIMEN FAILURES

The failure modes of the unjacketed specimens were as expected. For the ordinary tied columns, failure occurred suddenly due to cleavage of the concrete and simultaneous buckling of the longitudinal steel. Column Ref-Rect1/1-Ti44mm-ρ1.6, the square column with closely spaced ties, experienced cover spalling after which the load gradually decreased until the test was stopped because of excessive deformation in the column (see Figure 4.1). During testing of the spirally reinforced column, Ref-Circ-Sp51mm-ρ1.8, the load gradually increased after cover spalling until the spiral reinforcement ruptured. The difference in the behavior of Ref-Rect1/1-Ti44mm-ρ1.6 and Ref-Circ-Sp51mm-ρ1.8 can be attributed to how effectively the core of each column was confined. The post-spalling behavior of the two columns indicates that the spiral column was more effectively confined than the square column.

In all cases, the failure of the jacketed columns related directly to the rupture of the FRP jacket. The jacket ruptures ranged in width (measured along the longitudinal axis of the column) from 55 mm to 305 mm and tended to occur in the spaces between the steel ties. The widths of the ruptures were considerably smaller than the width of the individual fiber sheets, which were about 500 mm wide. In many instances, the jacket would rupture in small bands in one or more locations. Then, instead of the concrete simply continuing to crush in those unconfined areas, a large jacket rupture would occur somewhere along the length of the column and end the test. The failures of the columns with CFRP and AFRP jackets were notably more violent than the columns wrapped with GFRP and often even explosive. This trend is evident from the condition of the tested

specimens. Figure 4.2 through Figure 4.4 show specimens 2CFRP-Rect3/2-Ti178mm-ρ1.6, 2AFRP-Rect1/1-Ti178mm-ρ1.6, and 2GFRP-Rect1/1-Ti178mm-ρ1.6 after failure.

Figure 4.1. Ref-Rect1/1-Ti44mm-ρ1.6 After Testing

Figure 4.2. 305-mm Jacket Rupture on 2CFRP-Rect3/2-Ti178mm-ρ1.6

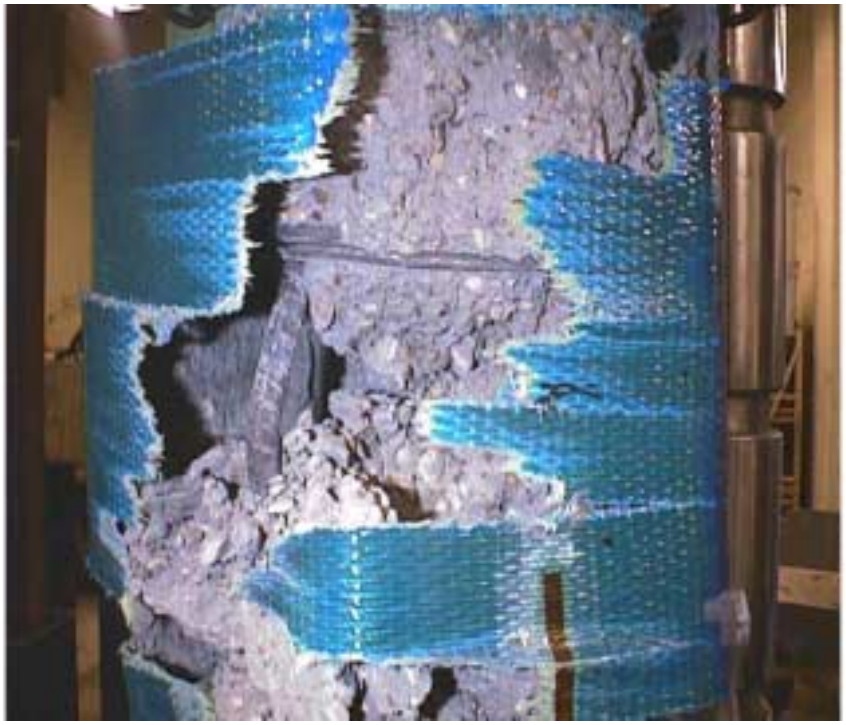

Figure 4.3. Close-up of 250-mm Jacket Rupture on 2AFRP-Rect1/1-Ti178mm-ρ1.6

Figure 4.4. 57-mm Jacket Rupture on 2GFRP-Rect1/1-Ti178mm-ρ1.6

The brittle failures of the jackets on the columns necessitated some modifications in the way in which the deformation of the columns were measured. The columns jacketed with aramid fibers and Ref-Rect1/1-Ti178mm-ρ1.6 were the first four columns to be tested. These columns were equipped with as many as seven LVDT's to measure lateral deflections and axial deformation at the midheight of the columns. Because these LVDT's were being damaged when the jackets ruptured, different measurement instruments had to be used. The remaining twenty-two columns were equipped with two string transducers (see Section 3.9 for further information) to measure axial deformation and a more durable type of LVDT. Only three of these LVDT's were available. One was used to measure axial deformation and the other two were used to measure lateral deflection. The two measuring lateral deflection were placed on opposite sides of the column. Placing them in this manner had the benefit of helping to discern what lateral movement was the result of bending and what movement was simply the sides of the rectangular columns bulging as the column was loaded. The drawback of having the

LVDT's on opposite sides of the column was that deflection in the perpendicular direction could not be monitored.

For non-circular columns, the carbon and glass jackets tended to fail at or near the corners. The aramid jackets failed primarily away from the corners on the specimens with one and two plies, but near the corner on the specimen with three plies. A thin layer of concrete was observed on the inside face of all of the failed jackets, demonstrating that good bond was achieved between the jacket and the column. Occasionally, however, some small areas of debond were noted between the putty and the jacket at the corners of the specimens. Some local buckling of the jackets was frequently observed on the non-circular columns along the faces between the corners.

Some of the jacketed columns showed visible curvature near the ultimate load stages. This may have been the result of a number of factors, including misaligned longitudinal reinforcing bars and accidental eccentricity in the axial load. Also, as mentioned previously, the slope of the axial-stress axial-strain curve of FRP-confined concrete becomes quite small in the latter load stages (see Figure 2.2 and accompanying discussion). This behavior leads to a propensity for second-order P-delta effects.

4.3. SPECIMEN COMPARISONS

4.3.1. General. Some graphical means of summarizing the performance of the columns will be helpful in ascertaining the effect of the various test variables. Two different types of figures have been constructed. One describes the ultimate axial stress sustained by the specimen, while the other shows the axial stress versus axial deformation data. The construction of each type of figure is discussed below.

4.3.2. Bar Charts of Normalized Ultimate Stress. The ultimate axial loads sustained by each of the columns are critical in determining the relative effect of each of the experimental variables. However, to make meaningful comparisons among the columns, the sustained loads must be normalized to account for the varying amounts

of longitudinal reinforcement and varying concrete strengths within the columns. The normalized ultimate stress is given by Equation 4.1,

$$\sigma_{n,ult} = \frac{P_{ult} - A_s f_y}{A_c f_c'} \qquad \text{Equation 4.1}$$

in which $\sigma_{n,ult}$ is the normalized ultimate stress, P_{ult} is the ultimate axial load, A_s is the area of the longitudinal reinforcement in the cross section, f_y is the yield strength of the longitudinal reinforcement, A_c is the area of concrete in the cross section and f'_c is the cylinder strength of the concrete. Equation 4.1 essentially subtracts the contribution of the longitudinal reinforcement from the sustained load for a given column and then divides this number by the contribution of the unconfined concrete. Thus, in a sense, $\sigma_{n,ult}$ is the ratio of the confined concrete strength to the unconfined concrete strength and measures how effectively the concrete is confined in a given cross section.

Some caution is warranted when interpreting the test results based on the normalized ultimate stress given in Equation 4.1. Note that the form of Equation 4.1 implies that the effect of the strength of the concrete in the column is to increase the ultimate capacity of the column in direct proportion to f'_c. This approximation is assumed to be valid because the variation in f'_c among the specimens is small. There are, however, some significant exceptions. In particular, note from Table 3.5 that columns numbered 3, 5, 11 and 20 through 23 had significantly weaker cylinder strengths than the average. Note also that columns numbered 4, 24, 25 and 26 had significantly stronger cylinder strengths than the average. The form of Equation 4.1 is such that larger normalized stresses result from lower concrete strengths for a given increase in the ultimate strength of the concrete in the column above f'_c. As an example, take two different FRP-jacketed columns. Suppose that for Column A f'_c is 20 MPa and that for Column B f'_c is 50 MPa. Now suppose that it was found that the ultimate stress in the concrete in each column was increased by 10 MPa over its respective f'_c value. The normalized ultimate stresses for Column A and Column B would then be 1.5 and 1.2, respectively. This difference in

$\sigma_{n,ult}$ appears despite the fact that an identical net increase in concrete strength was achieved in both columns.

Note that $\sigma_{n,ult}$ will not necessarily be equal to 1.0 for an unconfined column, since cylinder strengths are, in general, considerably greater than the compressive strength of the concrete in a column. In this study, the strength of the concrete in the unwrapped columns (excluding Ref-Circ-Ti178mm-ρ1.6, which was damaged, and Ref-Circ-Sp51mm-ρ1.8, which was confined by its transverse reinforcement) averaged about 88% of the strength of their respective cylinders. Thus, as one reviews the test results, the strength increase afforded by the FRP jackets should be viewed with respect to the normalized strength of the unwrapped columns and not to a normalized strength of 1.0.

Figure 4.5 is an example of one of several bar charts included in this report to show the variation of $\sigma_{n,ult}$ for various test parameters. Each bar is labeled along its left side with the descriptive name of the column that it represents. At the top of each bar is the value of $\sigma_{n,ult}$ for that particular column. It should be noted that special provision was made in determining $\sigma_{n,ult}$ for some specimens in order to account for strain hardening in the longitudinal steel. This will be discussed more fully later in the section. Special provision was also made for columns number 5 and 13 since the stress in the steel was less than the yielding stress when the load on the columns was greatest. In this case, $\sigma_{n,ult}$ was simply chosen as the greatest value on their respective normalized stress versus deformation curves. These curves are the second type of figure that will be used to compare the performance of the columns in this report. Their construction is described below.

4.3.3. <u>Normalized Stress Versus Deformation Curves</u>. In addition to ultimate stress values, useful inferences about the behavior of the columns can be made from the shape of the curves that trace their entire loading history. These curves have been plotted for various test parameters. For an example, see Figure 4.6. The horizontal axis shows axial deformation in microstrain. The vertical axis is the normalized axial

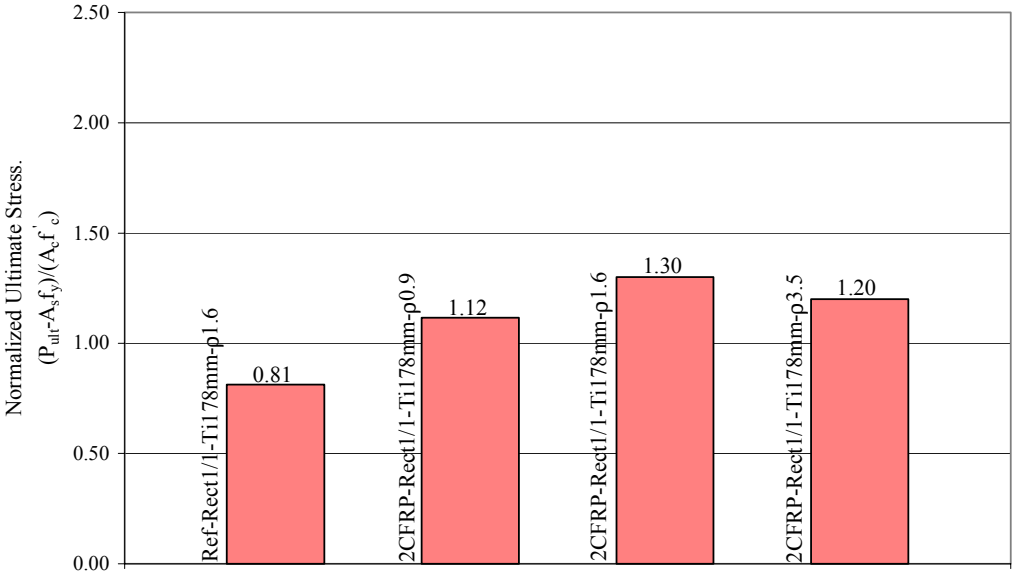

Figure 4.5. Comparison of Normalized Ultimate Stress (Variable Longitudinal Reinforcement Ratio)

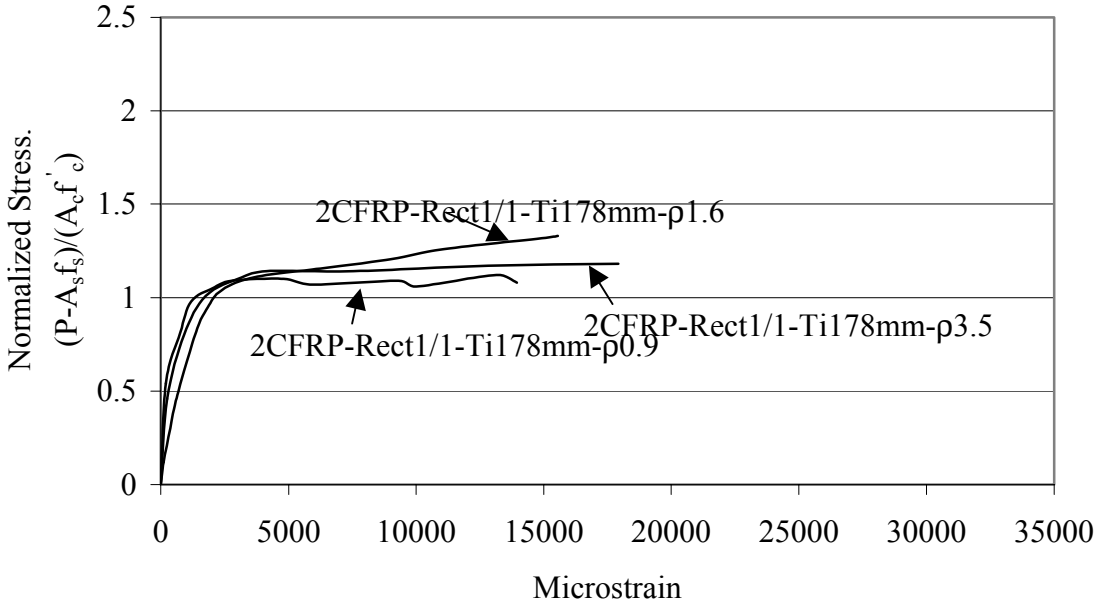

Figure 4.6. Comparison of Normalized Stress Versus Deformation (Variable

stress, which is computed in much the same way as the ultimate normalized stress in Equation 4.1. However, in this case P_{ult} is replaced by the axial load at a given load stage and f_y is replaced by the stress in the steel at that same load stage. The stress in the steel is computed by multiplying the axial deformation by an assumed modulus of 200 GPa. Perfectly plastic behavior is assumed after the steel yields (see Table 3.3 for f_y values) for all columns except those in which the effects of strain hardening are significant. These columns will be discussed more fully later in the section.

Some additional comments are in order about the manner in which the normalized stress versus deformation curves were constructed. First, there were several different instrument readings from which the axial deformations could be taken. As discussed in Section 3, axial deformation was measured by string transducers and LVDT's as well as by strain gages affixed to the FRP jackets and to the longitudinal steel. One benefit of using the strain gages rather than the LVDT's or string transducers is the much higher resolution of the strain gages, which results in smoother curves. A drawback, however, is that strain gages have small gage lengths and thus can measure only very localized deformations. After reviewing the available axial deformation data, it was determined that the string transducers and the LVDT's gave the most consistent and accurate results. These are the instruments from which the deformation data has been taken to plot the normalized stress versus deformation plots. The curves shown on the plots are actually the envelopes of the curves obtained during testing, since, as described in Section 3, the columns were subjected to a few loading cycles of increasing magnitude before they were loaded to failure. Showing only the envelope is necessary to prevent the plots from becoming unreadable as a result of excessive numbers of data points.

There are sometimes significant differences in the slopes of the curves in the elastic region, despite the fact that, ideally, they should be nearly identical. These differences can be attributed to three sources. First, as mentioned above, the deformation data for any one curve shown on a plot may be taken from either a string transducer or an LVDT. Inspection of the curves shows that the curves constructed from string transducer data tend to produce more steeply sloped elastic regions than the curves constructed from

LVDT data. This effect may be due to the difference in sensitivity and gage length between the two types of instruments, the LVDT being the most sensitive for its gage length and thus having a tendency to record more strain for a given load. The string transducers may have had a tendency to miss some axial deformation as a result of stretch in their strings or friction in the pulleys. Second, a smaller elastic slope in the raw load versus deformation data tends to be magnified when the data is normalized, because the effect of larger strains in the early load stages is to decrease the normalized stress, since larger strains produce greater steel stresses. Third, some of the differences in the elastic portions of the curves can be attributed to the differences in the strengths of the concrete in the various specimens. As a result of the normalization with respect to the y-axis, the stronger the concrete is, the smaller the slope of the normalized stress versus deformation curve is in the elastic region. Since this result may seem somewhat counterintuitive, it is explained below.

The slope of the elastic portion of the normalized curves is given by

$$E_n = \frac{\left(\frac{P - A_s f_s}{A_c f_c'}\right)}{\varepsilon_c} \qquad \text{Equation 4.2a}$$

$$= \frac{\left(\frac{P - A_s f_s}{A_c}\right)\left(\frac{1}{f_c'}\right)}{\varepsilon_c} \qquad \text{Equation 4.2b}$$

where E_n and ε_c are the slope of the normalized curve and the strain in the concrete, respectively. The bracketed left-hand term in the numerator of Equation 4.2b is the stress in the concrete, thus

$$E_n = \frac{(\sigma_c)\left(\frac{1}{f_c'}\right)}{\varepsilon_c} \qquad \text{Equation 4.3a}$$

$$= \left(\frac{\sigma_c}{\varepsilon_c}\right)\left(\frac{1}{f_c'}\right) \qquad \text{Equation 4.3b}$$

The left-hand term of Equation 4.3b is the modulus of elasticity of the concrete, so

$$E_n = \frac{E_c}{f_c'} \qquad \text{Equation 4.4}$$

where E_c is the modulus of elasticity of the concrete.

As established in the literature review, the effect of the FRP jacket is small in the elastic region, because the expansion of the concrete is small and thus little confining pressure is induced. We will assume that the moduli of the confined and unconfined concrete are identical in the elastic region. Then, using the well-know relationship that the modulus of elasticity of unconfined concrete is proportional to the square root of f'_c, the ratio of the slopes of two different curves becomes

$$\frac{E_{n1}}{E_{n2}} = \frac{\frac{\sqrt{f_{c1}'}}{f_{c1}'}}{\frac{\sqrt{f_{c2}'}}{f_{c2}'}} \qquad \text{Equation 4.5a}$$

$$\frac{E_{n1}}{E_{n2}} = \left(\frac{f_{c2}'}{f_{c1}'}\right)^{\frac{1}{2}} \qquad \text{Equation 4.5b}$$

Equation 4.5b shows that the ratio of the normalized slopes in the elastic region is inversely proportional to the square root of the concrete strengths, meaning that the stronger concrete will have the smaller slope on the normalized curve, as stated above. To summarize, Equation 4.2 through Equation 4.5 simply show that f'_c (a factor in the denominator of Equation 4.4) increases more quickly than E_c. Thus, the net effect of an increase in f'_c is a decrease in the slope of the normalized curve.

The effect of each of the test variables will now be examined with the aid of the two types of figures described above.

4.4. COMPARISON OF EFFECT OF TEST VARIABLES

4.4.1. Effect of Longitudinal Reinforcement. Figure 4.5 and Figure 4.6 show the effect of longitudinal reinforcement on the behavior of square columns with 2-ply CFRP jackets. Because the longitudinal steel was the variable in this comparison, strain hardening in the steel was considered in computing the normalized stresses. To make the comparisons between the columns more meaningful, these modified values are shown in Figure 4.5 and Figure 4.6. The modifications in the normalized stresses were made through the use of the stress versus strain curves obtained for the steel from tension tests. It should be noted that the strain hardening effects on 2CFRP-Rect$^{1}/_{1}$-Ti178mm-ρ3.5 had to be computed approximately, because the accuracy of the stress versus strain curve for the steel in this column was negatively affected by malfunctioning equipment. As it turned out, strain hardening reduced the ultimate normalized stress of 2CFRP-Rect1/1-Ti178mm-ρ1.6 from 1.33 to 1.30 and reduced 2CFRP-Rect1/1-Ti178mm-ρ3.5 from 1.42 to approximately 1.20, while 2CFRP-Rect1/1-Ti178mm-ρ0.9 remained unchanged at 1.12. Because the effect of strain hardening is small for 2CFRP-Rect1/1-Ti178mm-ρ1.6, it will not be considered in any of the figures other than Figure 4.5 and Figure 4.6. It should be noted that 2CFRP-Rect1/1-Ti178mm-ρ1.6 may have failed somewhat prematurely. Its jacket rupture at failure was a total of 305-mm wide, having a middle 165-mm portion which did not exhibit fiber fracture, but rather debonding at the lap splice where the fiber sheets had not been sufficiently saturated with resin and thus

pulled away from one another. However, given that the strength of 2CFRP-Rect1/1-Ti178mm-ρ1.6 is somewhat larger than 2CFRP-Rect1/1-Ti178mm-ρ3.5, it is unlikely that the strength of 2CFRP-Rect1/1-Ti178mm-ρ1.6 was significantly reduced by the lap splice failure.

4.4.2. Effect of Corner Sharpness. Figure 4.7 and Figure 4.8 show the effect of corner sharpness on the behavior of square cross sections confined with 2-ply CFRP jackets. The trend is clearly an increase in ultimate strength with decreasing corner sharpness. Note in Figure 4.8 that there is a drop in the curve of 2CFRP-Rect1/1-Ti178mm-ρ1.6-19mm between about 16,500 microstrain and 18,300 microstrain. This sudden increase in strain and slight load drop corresponded to a 51-mm-wide jacket rupture that initiated at a point where the jacket was inadvertently damaged prior to the test. The end of the curve corresponds to a 130-mm-wide rupture that occurred directly below the initial rupture and ended the test. Note that the curve for 2CFRP-Rect1/1-Ti178mm-ρ1.6-6.4mm descends immediately after the transition zone, but then begins to increase at approximately the same rate as the other two curves. This shape suggests behavior similar to that described by Picher et al. (1996), who stated that large strains in the lateral direction cause deformation of a square cross section into a more rounded geometry that helps the jacket to be more effective. This increase in confinement effectiveness may be what caused the curve of the sharp-cornered column to begin to ascend shortly before failure.

4.4.3. Effect of Tie Spacing (Circular Cross Sections). Figure 4.9 and Figure 4.10 show the effect of tie spacing on columns with circular cross sections. Ref-Circ-Ti178mm-ρ1.6 would have been included in these figures, except that severe honeycombing on the column unfavorably impacted the results of its test. Its ultimate normalized stress reached only 0.56.

Note the relatively steep slope of 1CFRP-Circ-Sp51mm-ρ1.8 in the plastic zone, indicating good confinement from the combination of the steel spiral and CFRP jacket.

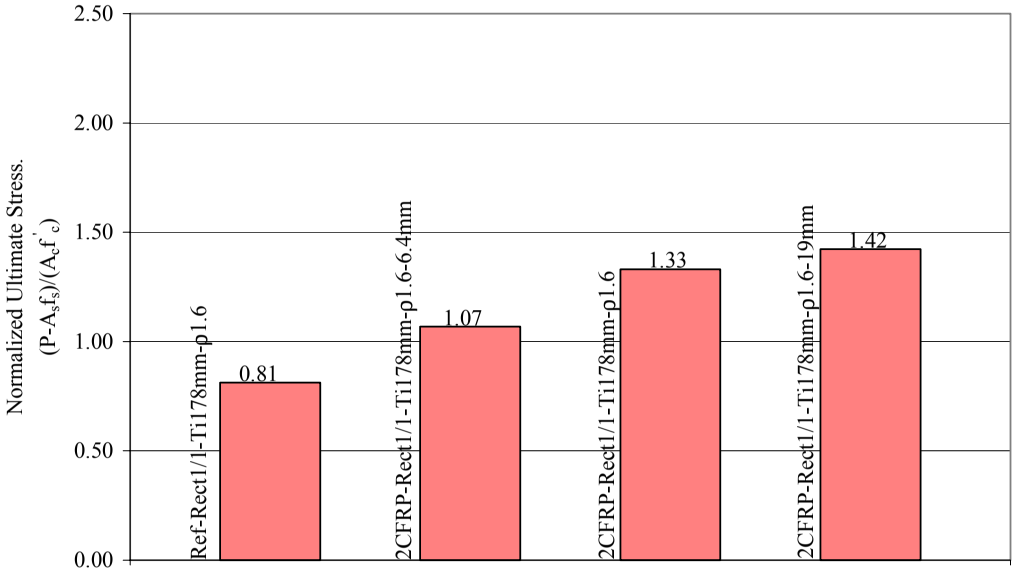

Figure 4.7. Comparison of Normalized Ultimate Stress (Variable Corner Sharpness)

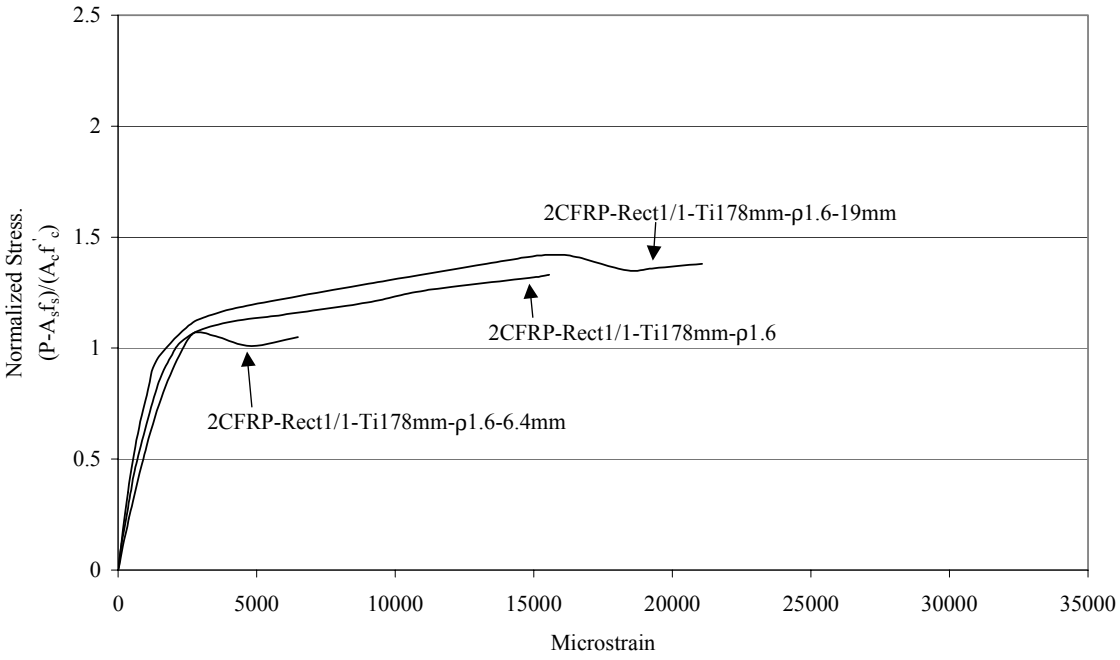

Figure 4.8. Comparison of Normalized Stress Versus Deformation (Variable Corner Sharpness)

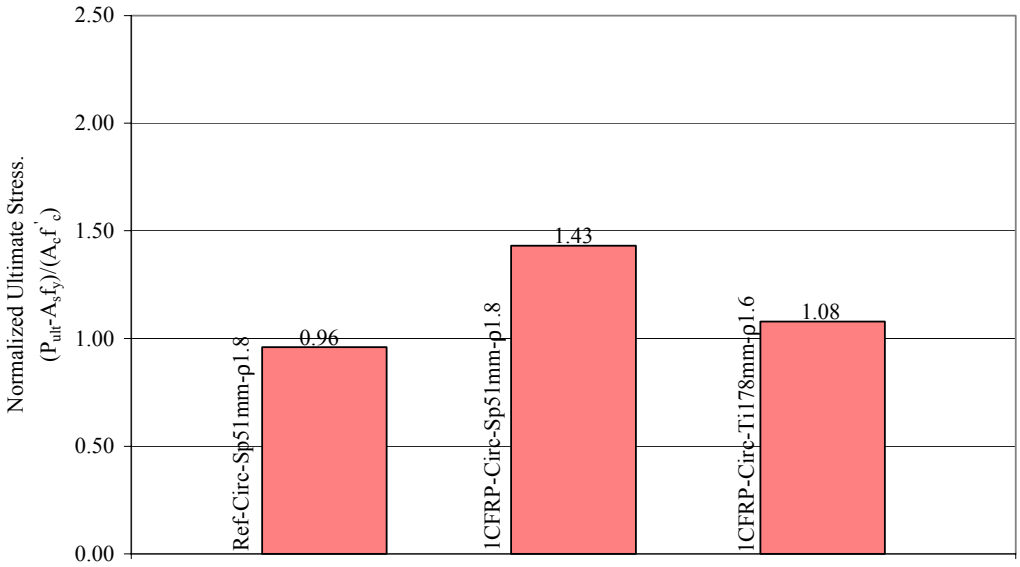

Figure 4.9. Comparison of Normalized Ultimate Stress (Circular Cross Section, Variable Tie Spacing)

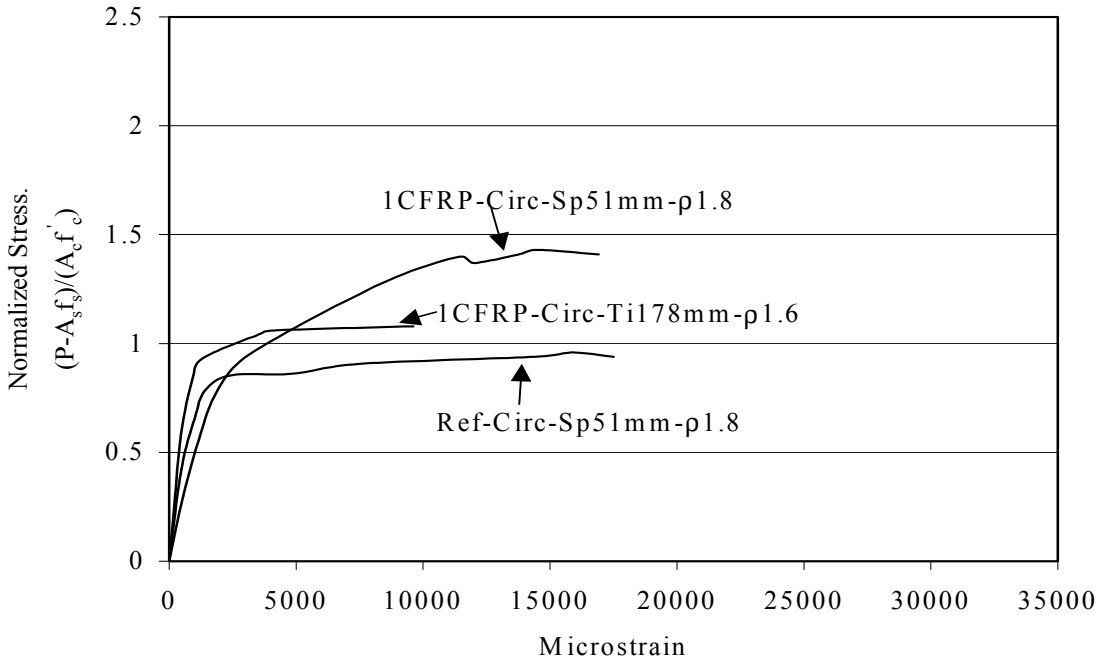

Figure 4.10. Comparison of Normalized Stress Versus Deformation (Circular Cross Section, Variable Tie Spacing)

The failure of this column is noteworthy. As it was being loaded, a large jacket rupture approximately 165 mm wide occurred at the bottom of the column. However, the spiral reinforcement did not rupture at this location. Instead, the load resistance of the column dropped to about 85% of the ultimate strength of its unjacketed counterpart, Ref-Circ-Sp51mm-ρ1.8. At this point, another major jacket rupture, this time with a simultaneous spiral rupture, occurred near the middle of the specimen and ended the test. Figure 4.10 shows only the portion of the curve up to the first jacket rupture, as after this point the axial deformation data is not available.

4.4.4. Circular Versus Square Cross Sections. Figure 4.11 and Figure 4.12 show the behavior of a circular and a square column, each having a 1-ply CFRP jacket. It is not clear why the square section sustained a greater axial normalized stress than the circular section. However, the larger axial strain that the square section sustained may be the result of the section's tendency to deform to a slightly more rounded shape as it is being loaded. This new, more rounded section would have greater area, allowing the column to compress axially to fill the expanded section.

4.4.5. Effect of Tie Spacing (2.0 Aspect Ratios). Figure 4.13 and Figure 4.14 display the effect of tie spacing on specimens having aspect ratios of 2.0 and wrapped with 2-ply CFRP jackets. Note that Ref-Rect2/1-Ti127mm-ρ1.6 has a much smaller ultimate strength and, as shown in Figure 4.14, a smaller slope than Ref-Rect2/1-Ti178mm-ρ1.6. The differences here may be the result of a larger eccentricity for the load on Ref-Rect2/1-Ti127mm-ρ1.6, as the LVDT's measuring lateral movement recorded about 2.8 mm of deflection at the ultimate load for this column, while they recorded only 0.254 mm for Ref-Rect2/1-Ti127mm-ρ1.6. The differences between the slopes of the jacketed columns and Ref-Rect2/1-Ti178mm-ρ1.6 can be attributed mainly to the fact that string transducer data is shown for the jacketed columns, while LVDT data is shown for Ref-Rect2/1-Ti178mm-ρ1.6. The two jacketed columns are similar in ultimate strength, but 2CFRP-Rect2/1-Ti127mm-ρ1.6 sustained more deformation.

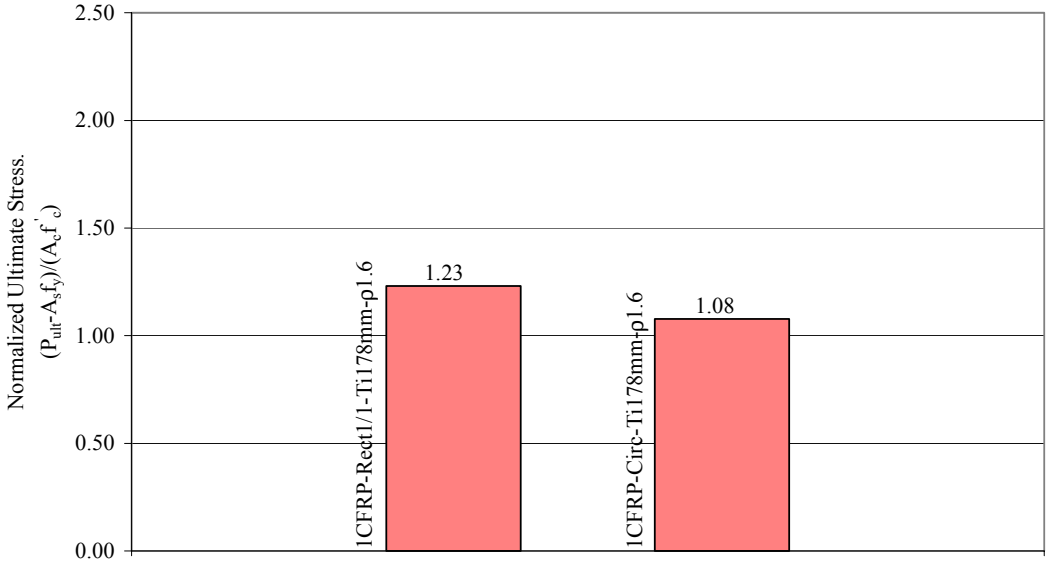

Figure 4.11. Comparison of Normalized Ultimate Stress (Circular Versus Square Cross Section)

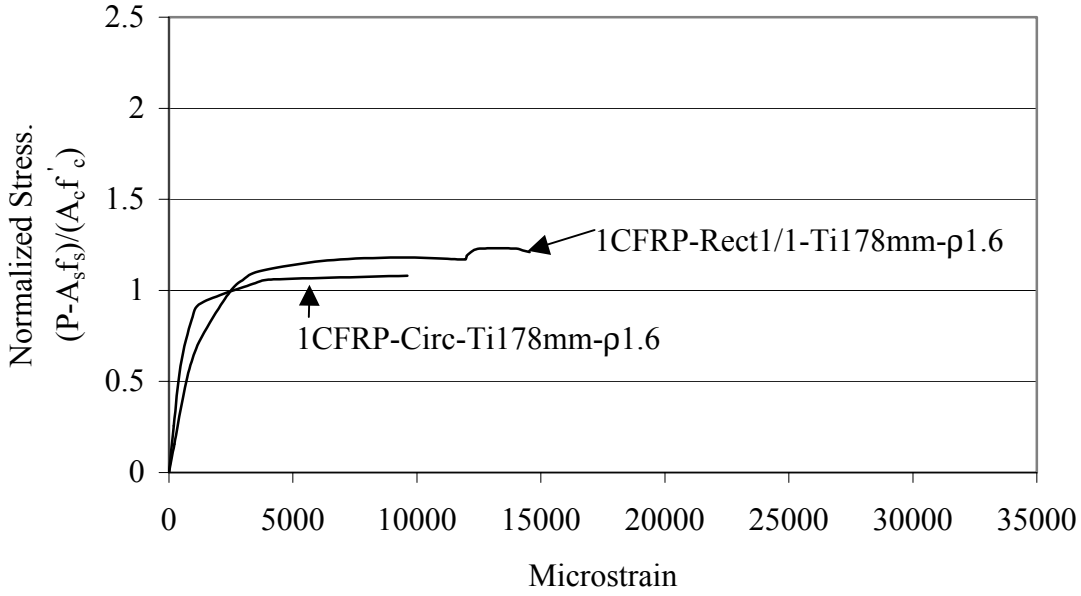

Figure 4.12. Comparison of Normalized Stress Versus Deformation (Circular Versus Square Cross Section)

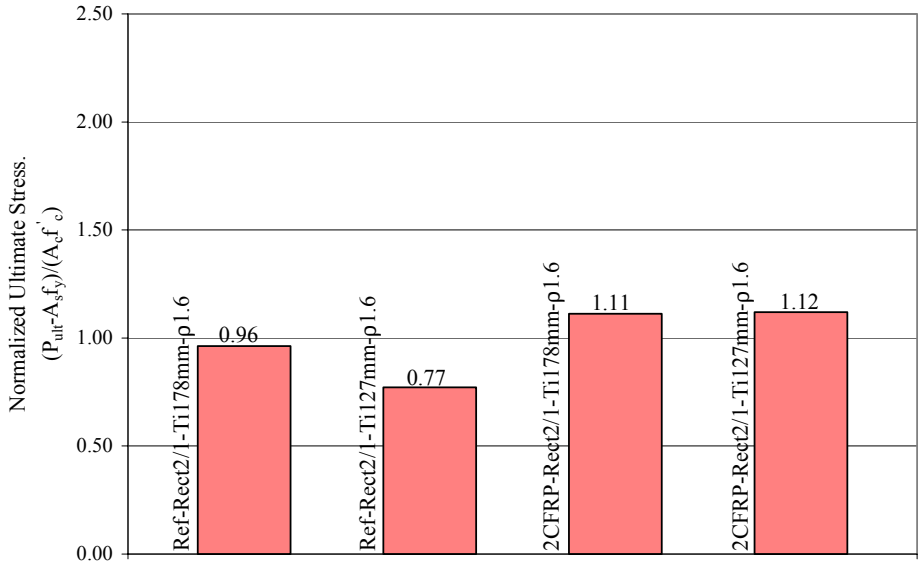

Figure 4.13. Comparison of Normalized Ultimate Stress (2.0 Cross-Sectional Aspect Ratio, Variable Tie Spacin

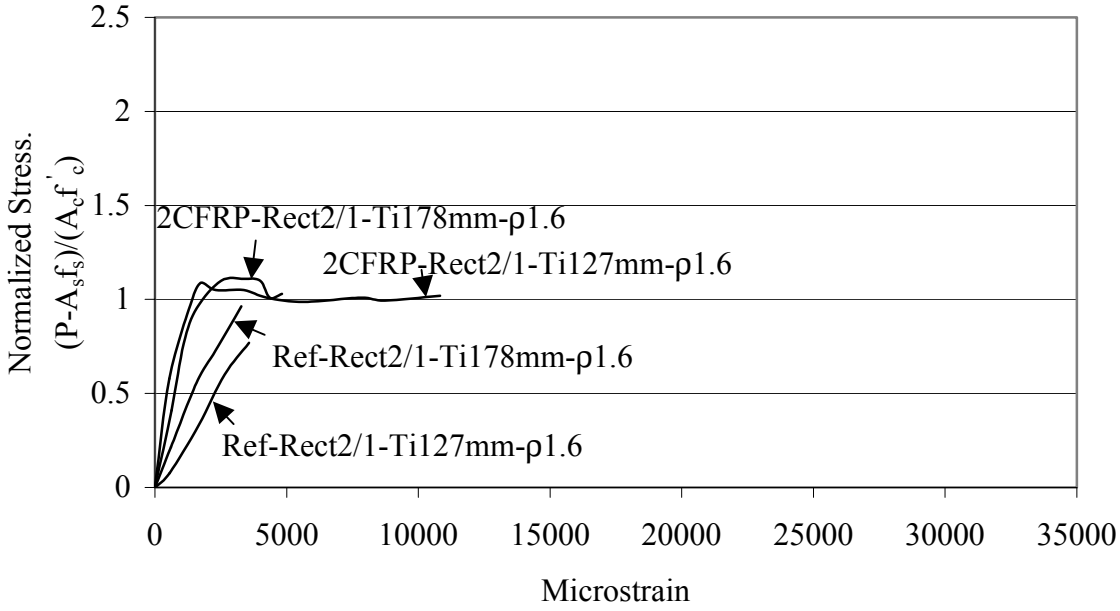

Figure 4.14. Comparison of Normalized Stress Versus Deformation
(2.0 Cross-Sectional Aspect Ratio, Variable Tie Spacing)

4.4.6. Effect of Tie Spacing (Square Cross Sections). Figure 4.15 and Figure 4.16 show the effects of tie spacing on square cross sections with 2-ply CFRP jackets. It is important to keep in mind that the slopes of the elastic portions of the curves in Figure 4.16 are different for the reasons discussed previously, and not as a result of actual stiffness changes brought about by the variation in the test parameters. As would be expected, Ref-Rect1/1-Ti44mm-ρ1.6 shows greater ultimate axial deformation and greater ultimate strength than Ref-Rect1/1-Ti178mm-ρ1.6. It is difficult to reconcile the unusually low strength of 2CFRP-Rect1/1-Ti102mm-ρ1.6. No unusual failure characteristics were noted during testing for this column and the readings from the LVDT's measuring lateral deflection were similar for all three of the jacketed columns. Also, all three of the jacketed columns shown were cast from the same concrete pour, eliminating any differences that may have been the result of normalizing with respect to f'_c. Note that the behavior of 2CFRP-Rect1/1-Ti44mm-ρ1.6 differs significantly from 1CFRP-Circ-Sp51mm-ρ1.8. Figure 4.10 shows that for 1CFRP-Circ-Sp51mm-ρ1.8 the combined effect of steel and FRP confinement resulted in a significant increase in the slope of the plastic portion of the curve over that of the specimens confined by only FRP or only steel. Figure 4.16 shows that the combined steel and FRP confinement for the square cross section resulted in approximately the same slope in the plastic portion of its curve as the two jacketed columns with larger tie spacings. However, the axial strain sustained by 2CFRP-Rect1/1-Ti44mm-ρ1.6 is larger than for the other specimens. Some comment on the failure of 2CFRP-Rect1/1-Ti44mm-ρ1.6 is in order. After the jacket ruptured, it behaved much like its unjacketed counterpart, Ref-Rect1/1-Ti44mm-ρ1.6, in that the ties never ruptured, and its resistance to loading slowly decreased until the test was stopped. Figure 4.16 shows the behavior of the column only up to jacket rupture.

4.4.7. Effect of Aspect Ratio. Figure 4.17 and Figure 4.18 show the effect of the cross-sectional aspect ratio on rectangular columns wrapped with 2-ply CFRP jackets. Increasing aspect ratios led to decreased ultimate strengths. Larger aspect ratios also resulted in smaller ultimate strain values, though the small ultimate strain value for the column with the 2.0 aspect ratio may be somewhat misleading. Recall from Figure 4.14

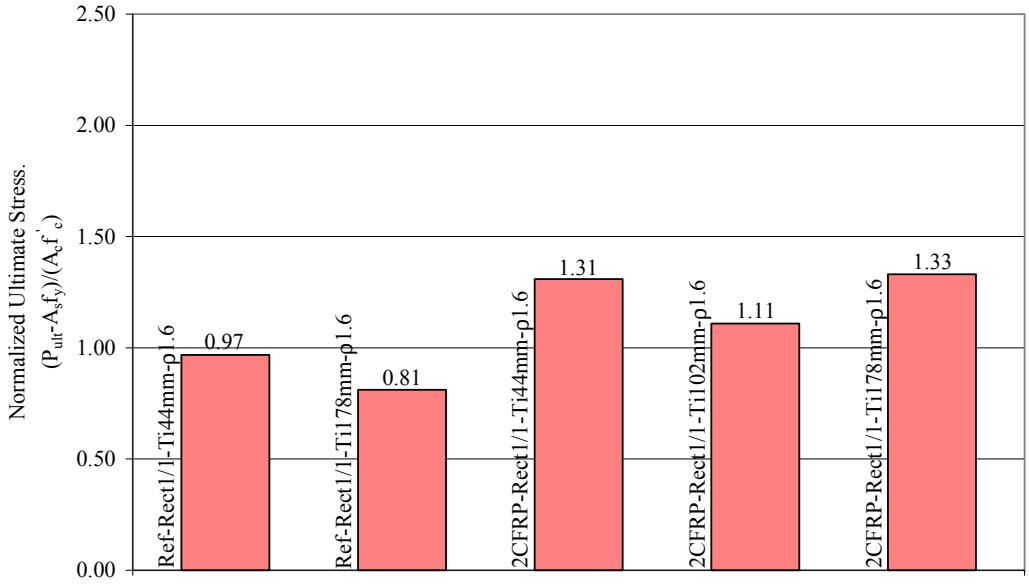

Figure 4.15. Comparison of Normalized Ultimate Stress (Square Cross Section, Variable Tie Spacing)

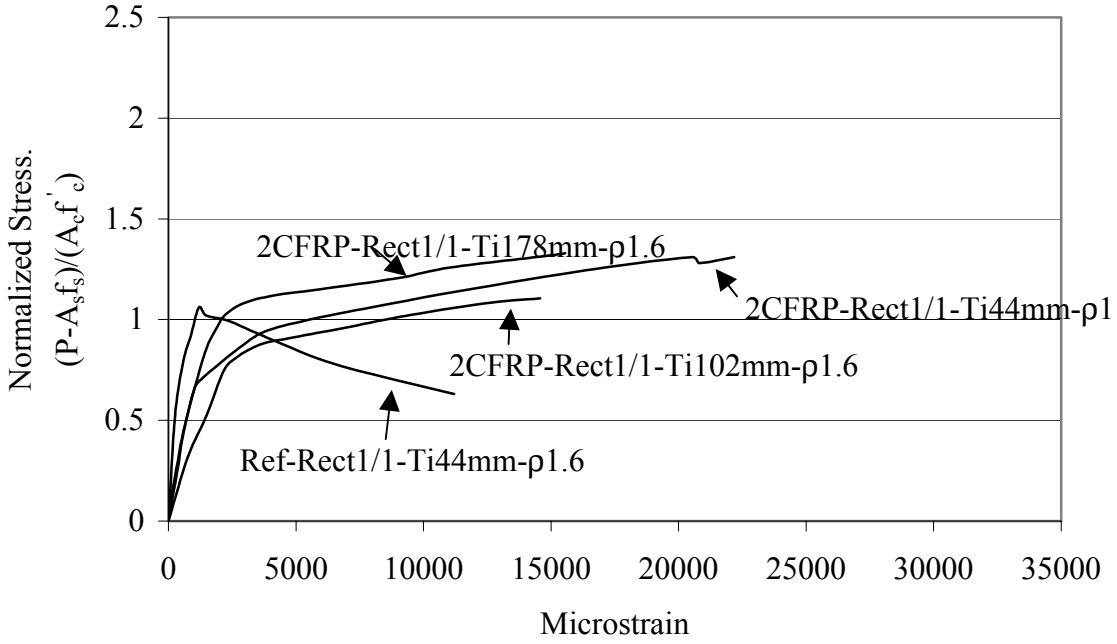

Figure 4.16. Comparison of Normalized Stress Versus Deformation (Square Cross Section, Variable Tie Spacing)

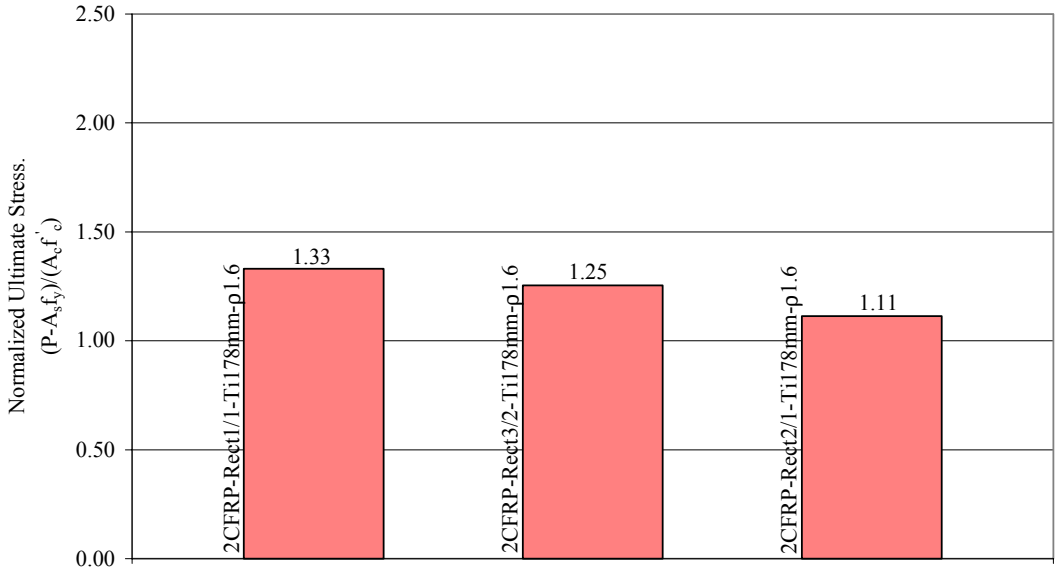

Figure 4.17. Comparison of Normalized Ultimate Stress (Variable Aspect Ratio)

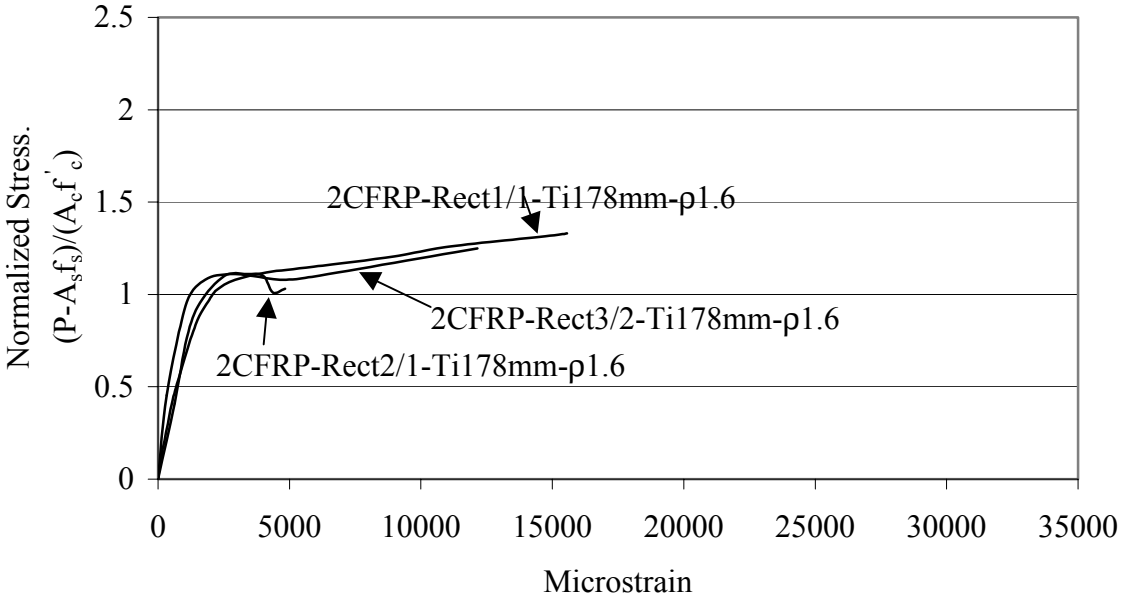

Figure 4.18. Comparison of Normalized Stress Versus Deformation (Variable Aspect Ratio)

that 2CFRP-Rect2/1-Ti127mm-ρ1.6 sustained approximately 10,800 microstrain. Note the differences in the slopes of the plastic regions of the specimens. 2CFRP-Rect2/1-Ti178mm-ρ1.6 had a descending curve, while the ascending slopes of 2CFRP-Rect1/1-Ti178mm-ρ1.6 and 2CFRP-Rect3/2-Ti178mm-ρ1.6 are nearly identical. The identical slopes indicate that the concrete in both columns was experiencing approximately the same confinement. Thus, the difference in strength between the two specimens does not appear to be the result of differences in the confinement of the section for a given load, but rather differences in the jacket distress caused by a given load. The 1.5 aspect ratio caused more distress for a given load than the 1.0 aspect ratio and thus forced failure of the jacket more quickly.

4.4.8. The 1.5 Aspect Ratio. Figure 4.19 and Figure 4.20 show the increase in strength and deformation provided by two plies of CFRP on a rectangular column with an aspect ratio of 1.5. The increase in strength is about 37%, which falls between the increases in strength observed for similar pairs of columns having aspect ratios of 1.0 and 2.0. In particular, the increase in strength between Ref-Rect$^{1}/_{1}$-Ti178mm-ρ1.6 and 2CFRP-Rect$^{1}/_{1}$-Ti178mm-ρ1.6 was 64% (see Figure 4.15), while the increase in strength between Ref-Rect$^{2}/_{1}$-Ti178mm-ρ1.6 and 2CFRP-Rect$^{2}/_{1}$-Ti178mm-ρ1.6 was 16% (see Figure 4.13).

4.4.9. Effect of CFRP Jacket Thickness. Figure 4.21 and Figure 4.22 show the strengthening effects of the number of plies of CFRP applied to square columns. Note that the ultimate strength of the column with 1 ply of CFRP is only about 7.5% less than the strength of the column with 2 plies. This small difference in ultimate normalized strength may partially be due to the relatively small cylinder strength of the 1-ply specimen. As discussed in Section 4.3.2, small cylinder strengths tend to produce large normalized ultimate strengths.

4.4.10. Effect of AFRP Jacket Thickness. Figure 4.23 and Figure 4.24 show the strengthening effect of various numbers of plies of AFRP on square columns. As

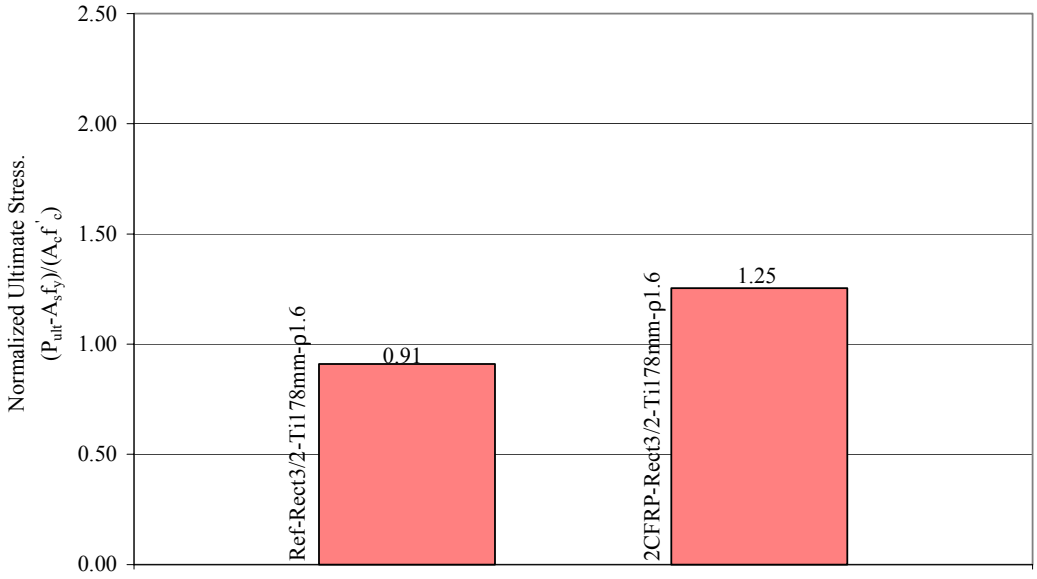

Figure 4.19. Comparison of Normalized Ultimate Stress (3/2 Aspect Ratio)

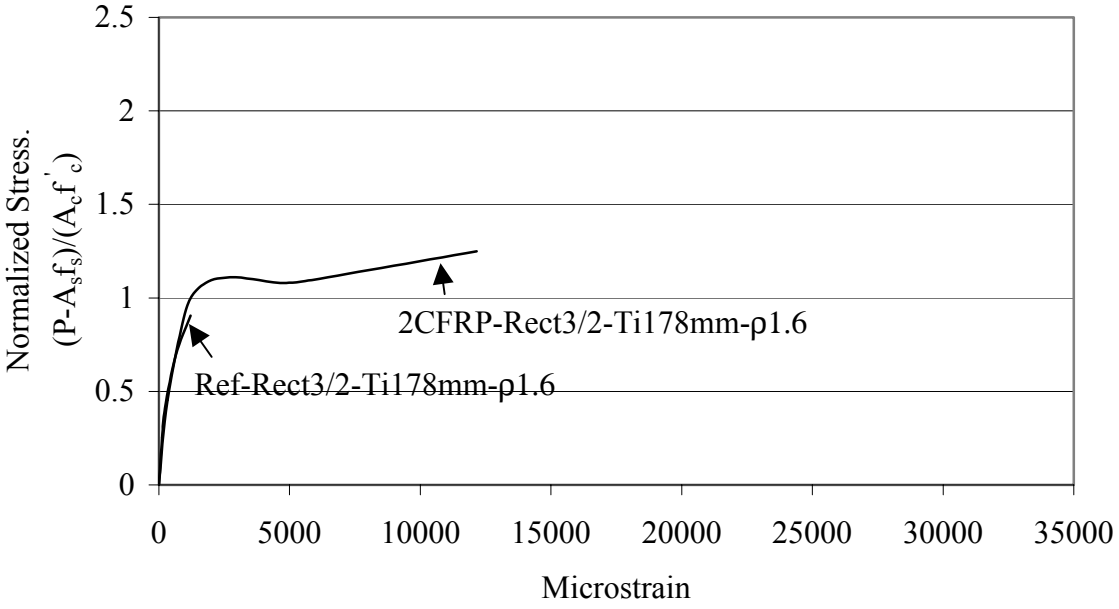

Figure 4.20. Comparison of Normalized Stress Versus Deformation (3/2 Aspect Ratio)

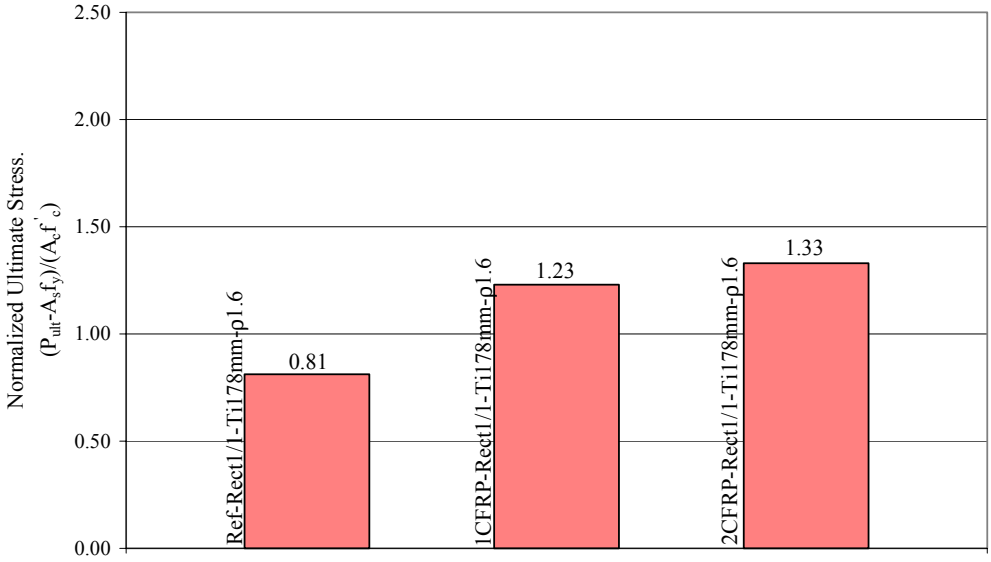

Figure 4.21. Comparison of Normalized Ultimate Stress (Variable CFRP Jacket Thickness)

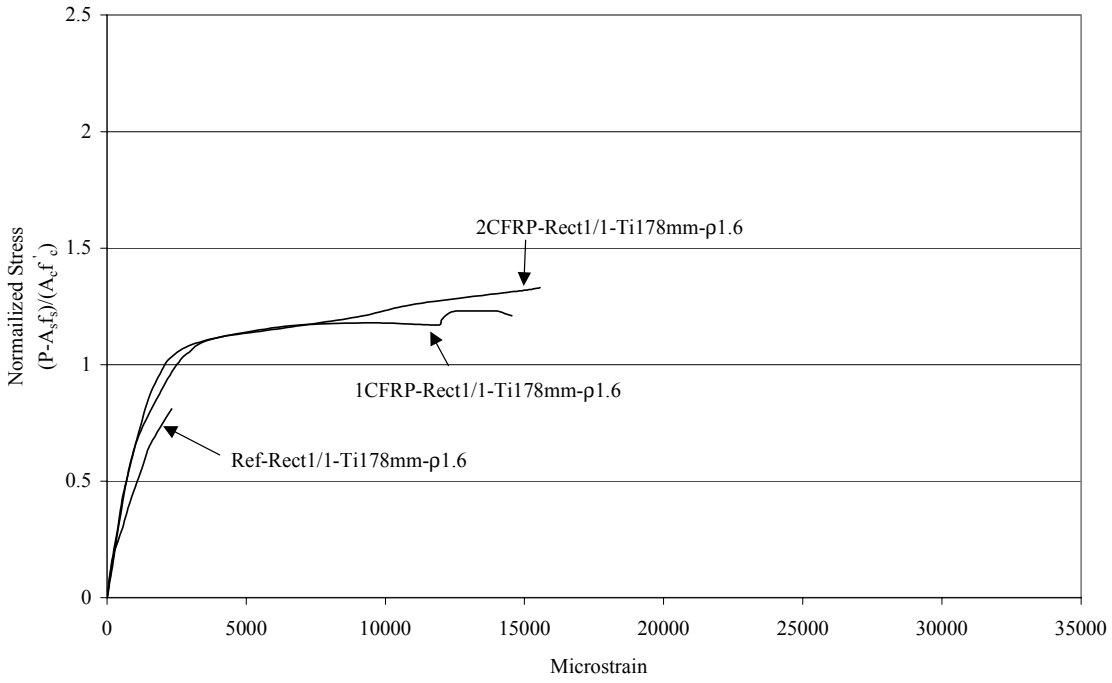

Figure 4.22. Comparison of Normalized Stress Versus Deformation (Variable CFRP Jacket Thickness)

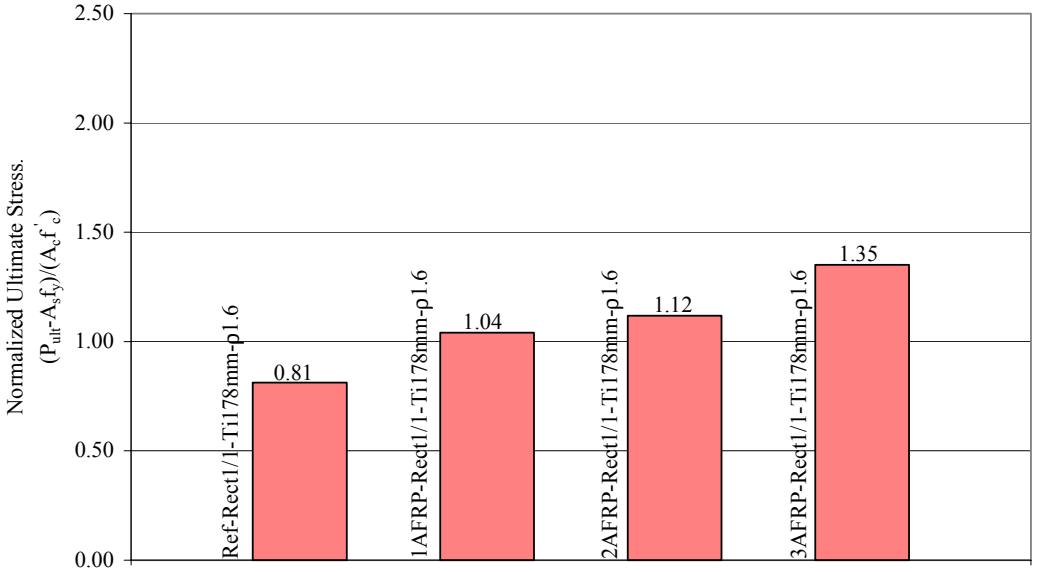

Figure 4.23. Comparison of Normalized Ultimate Stress (Variable AFRP Jacket Thickness)

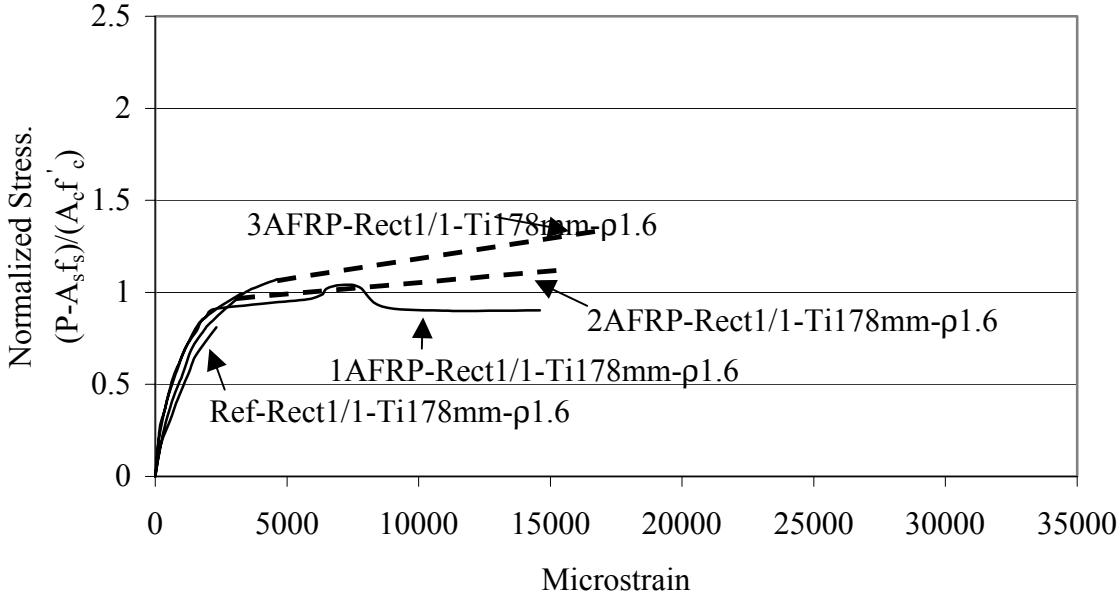

Figure 4.24. Comparison of Normalized Stress Versus Deformation
(Variable AFRP Jacket Thickness)

with the CFRP jackets, increasing plies results in increasing ultimate strength. In Figure 4.24 the deformation data for the 2-ply and 3-ply specimens is not available beyond the transition zone, so straight lines have been added that extend to the appropriate ultimate strength value. Note that since the ultimate axial strain values are not known, the actual slopes of the lines may be somewhat different from what is shown.

4.4.11. Effect of GFRP Jacket Thickness. Figure 4.25 and Figure 4.26 show the strengthening effect of various numbers of plies of GFRP on square columns. The GFRP appears to be more effective than the AFRP at confining the columns, exhibiting both greater ultimate normalized strength and axial deformation for a given number of plies. However, the 1-ply GFRP jacket did not cause as great a strength increase as the 1-ply CFRP jacket, though the 1-ply GFRP specimen did sustain more axial deformation.

4.4.12. Net Increase in Concrete Strength. As discussed in Section 4.3.2, $\sigma_{n,ult}$ (see Equation 4.1) may give normalized stresses that are somewhat biased when large differences in f'_c exist between the columns that are being compared. Since the differences in f'_c between the columns with the three fiber types is rather large (see Table 3.5), Figure 4.27 was constructed as an alternate way to view the confinement effectiveness of the three fiber types. Figure 4.27 is a bar chart that shows the difference between the ultimate confined concrete stress and the unconfined cylinder strength of the concrete for specimens with 2-ply jackets of carbon, aramid and glass. The trend in Figure 4.27 is similar to the trend seen in Figure 4.21, Figure 4.23 and Figure 4.25. The ranking of the fiber types from the greatest concrete strength increase to the smallest is GFRP, CFRP and then AFRP. Interestingly, this order is different from the actual tensile strength of the sheets. Table 3.4 shows that the ranking of the fiber sheets from the greatest tensile strength to the smallest is CFRP, AFRP and then GFRP.

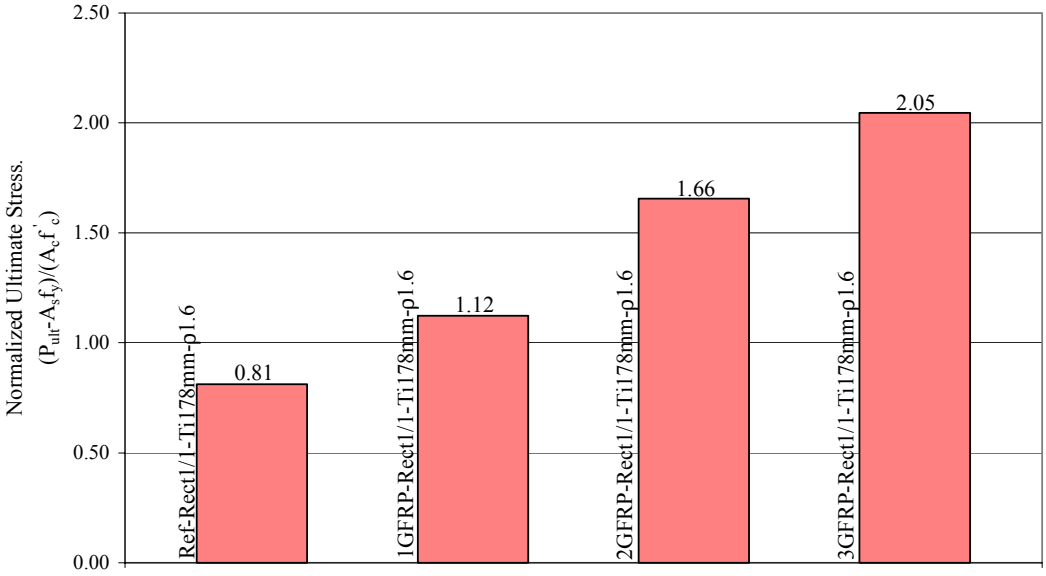

Figure 4.25. Comparison of Normalized Ultimate Stress (Variable GFRP Jacket Thickness)

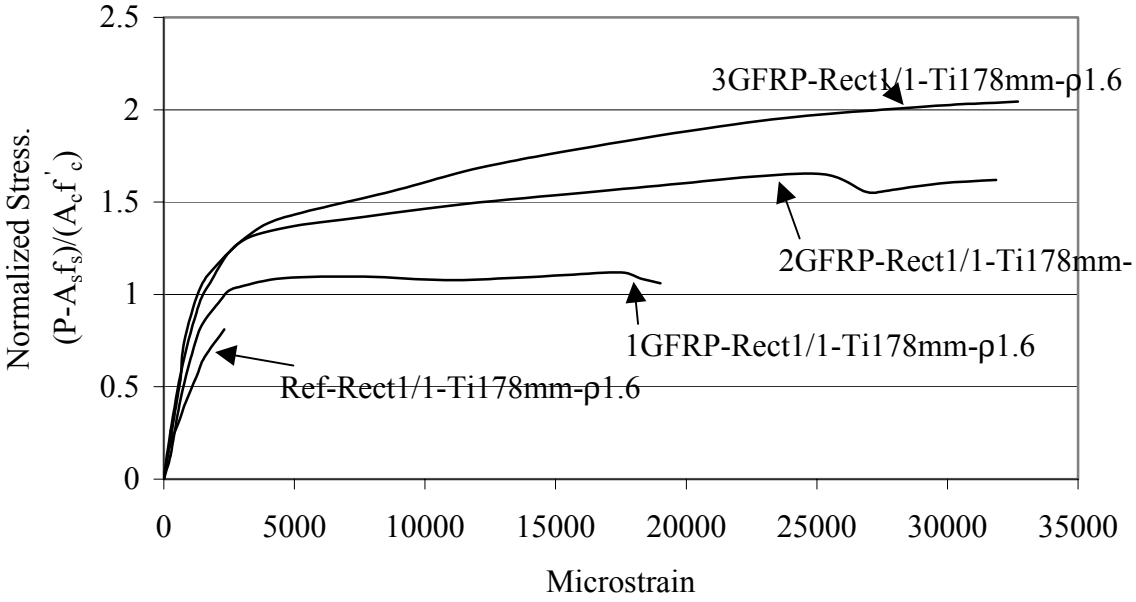

Figure 4.26. Comparison of Normalized Stress Versus Deformation
(Variable GFRP Jacket Thickness)

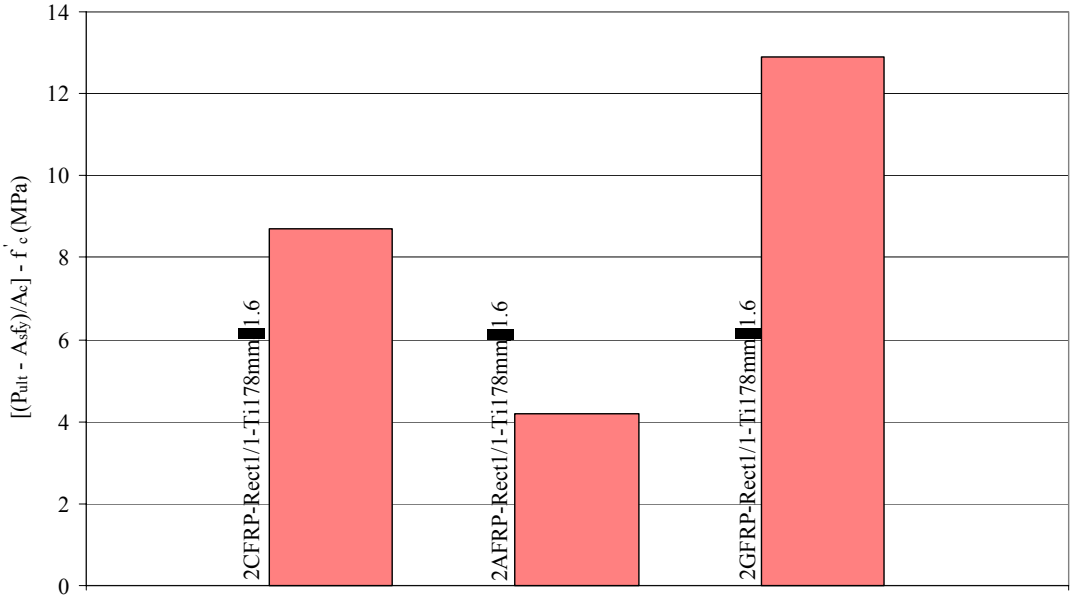

Figure 4.27. Comparison of Net Increase in Concrete Strength for 2-ply Jackets on Square Columns

4.5. COMPARISON OF HOOP JACKET STRAINS

4.5.1. General. The hoop strain in a jacket, as measured by the strain gages applied to the surface of the jacket (see Figure 3.8e), is an important indicator of the performance of the jacket. The purpose of this section is to describe the behavior of the jacket in order to give a better understanding of how it acts as a confinement mechanism. Some comments are in order about the variables that may have affected the jacket strain data presented in this section. First, the jacket strain readings can be affected by the proximity of the gage to one of the steel ties used as internal transverse reinforcement. This effect has not been accounted for in this study. Second, the jacket strain readings can be affected by the thickness of the jacket at a particular position on the column. Recall from Section 3 that the jackets were constructed from sheets of fiber saturated in resin and overlapped at their ends to provide for the development of the fiber. These overlapped areas cause non-uniform jacket thickness around the perimeter of the column cross section. The effect of this variable jacket thickness on the jacket strain has not been considered in this study.

4.5.2. Jacket Strain at Different Load Stages. Figure 4.28 shows the hoop strain at three locations on the jacket of 2CFRP-Rect1/1-Ti178mm-ρ1.6 for three load stages. The strains shown in this figure, as well as in similar proceeding figures, are the larger of the two strains recorded for a particular position on the jacket. This column is given as a representative of typical jacket behavior. Note that the jacket sustains very little strain until the load reaches the ultimate capacity of the column. This is to be expected, since, as discussed previously, the column cross section does not begin to react against the restraint of the jacket until the latter load stages. In Figure 4.28 and in similar figures that follow, the ultimate condition refers to the jacket strain at jacket rupture and not necessarily at the instant when the largest axial load was applied, though these points often coincide. However, in Figure 4.28 "1/2 ultimate" and "3/4 ultimate" refer to the jacket strain at 50% and 75%, respectively, of the largest axial load sustained by the column. In the following discussion, the positions "corner", "half-face" and "quarter-face" refer to the corner, the midpoint between the corners and the point that is one-fourth

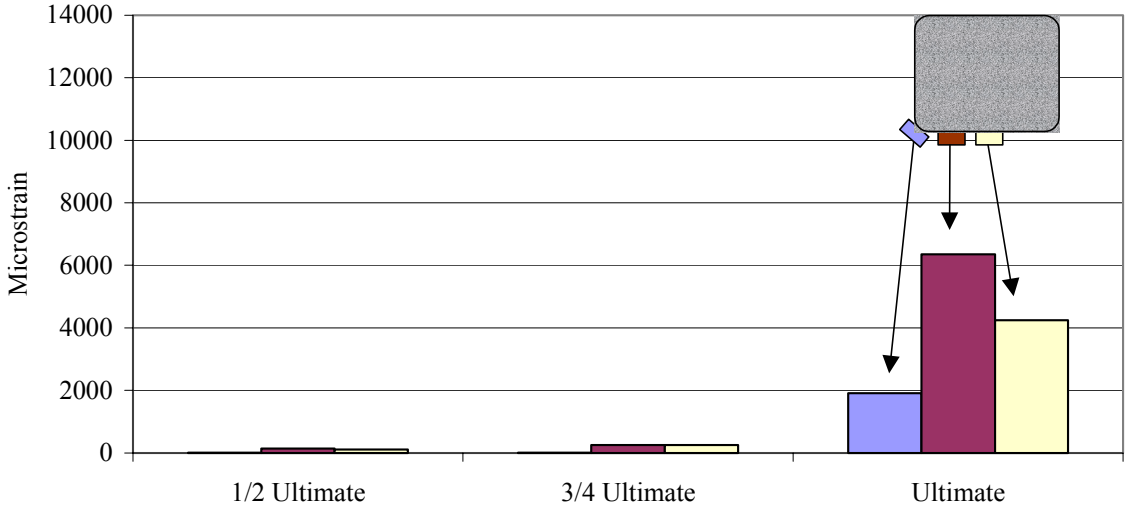

Figure 4.28. Hoop Jacket Strain at Different Load Stages (2CFRP-Rect1/1-Ti178mm-ρ1.6)

the distance between the corners along the face of the column, respectively. These positions are shown graphically at the top right-hand portion of Figure 4.28.

4.5.3. Jacket Strain at Fracture. The data indicate that adverse variables (for example, sharp column corners or large cross-sectional aspect ratios) force jacket failure to occur at low jacket strains. Figures 4.29 and 4.30 show the jacket strain at the ultimate for the columns with variable corner sharpness and cross-sectional aspect ratios. It is clear from these figures that the axial strain in the fibers as measured by the strain gages is not a good indicator of the point of jacket rupture, since, if this were the case, all the jackets would have failed at similar strain levels. Instead, what is shown is that the adverse variables actually force failure at smaller jacket strains. Note that larger jacket strains indicate that the column is experiencing better confinement, since the jackets that sustained greater strain were on the columns that sustained the greatest axial loads and axial deformations (compare Figure 4.8 with Figure 4.29 and also Figure 4.18 with Figure 4.30). Thus it appears that larger axial fiber strains in a jacket are predominantly the result of more effective confinement applied to the column, rather than stress concentrations caused by adverse variables.

4.5.4. Variability of Jacket Strain with Position. It can be seen in Figure 4.28 through Figure 4.30 that there are significant differences in the strain in the jacket at the three locations where strain gages were applied. In fact, it can be seen that the corner gages showed consistently smaller strains than either the quarter-face or the half-face gages. However, as mentioned previously, it was noted during testing that the jacket failures tended to occur at the corners. To explain this apparent discrepancy, recall from the above discussion that the axial strain may not be a good indicator of the failure of the jacket. Also, consider Figure 4.31, which shows the profile of the cross section of a jacketed column before and after loading. As a result of the curvature of the jacket during loading, flexural stresses can be induced in the jacket. The deformed shape of the jacket is such that flexural tension would result at the half-face strain gage and flexural compression at the corner stain gage. These flexural stresses, when superimposed on the

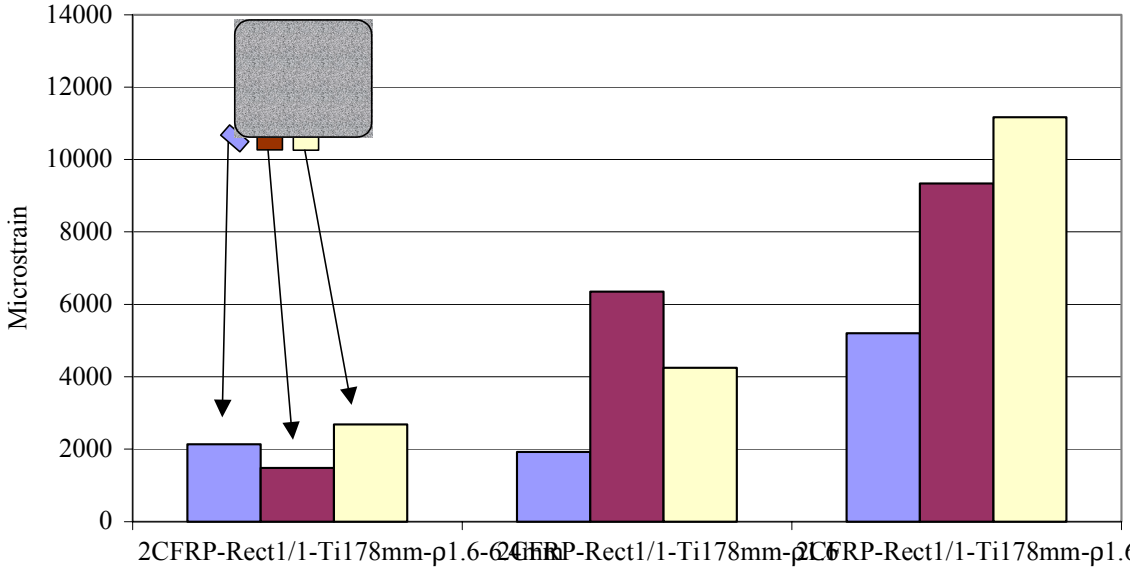

Figure 4.29. Ultimate Hoop Jacket Strain (Variable Corner Sharpness)

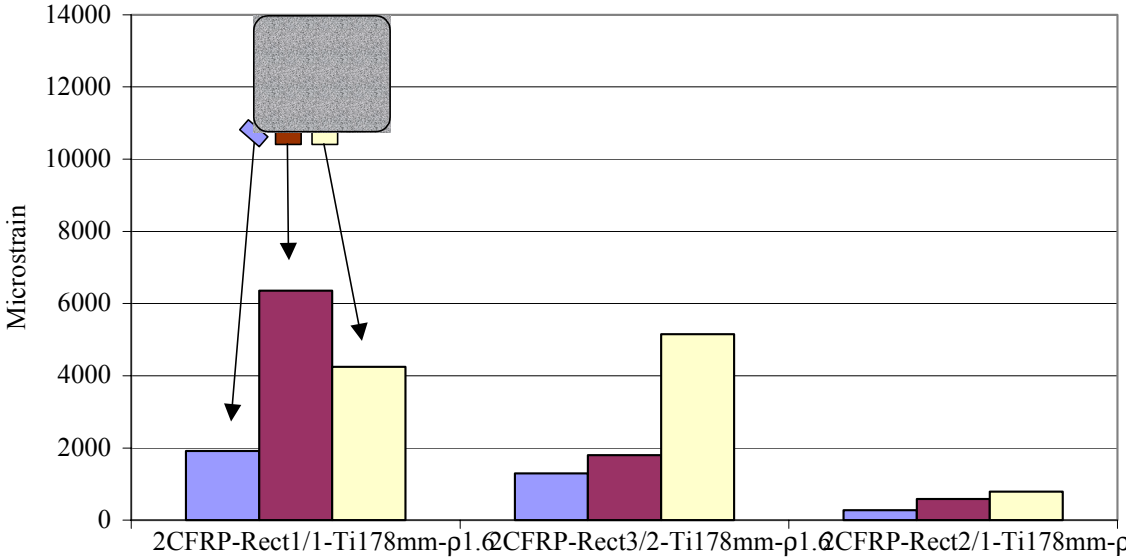

Figure 4.30. Ultimate Hoop Jacket Strain (Variable Apect Ratio)

tensile stresses that occur because of the confining pressure, would result in higher strain readings at the half-face strain gage than at the corners.

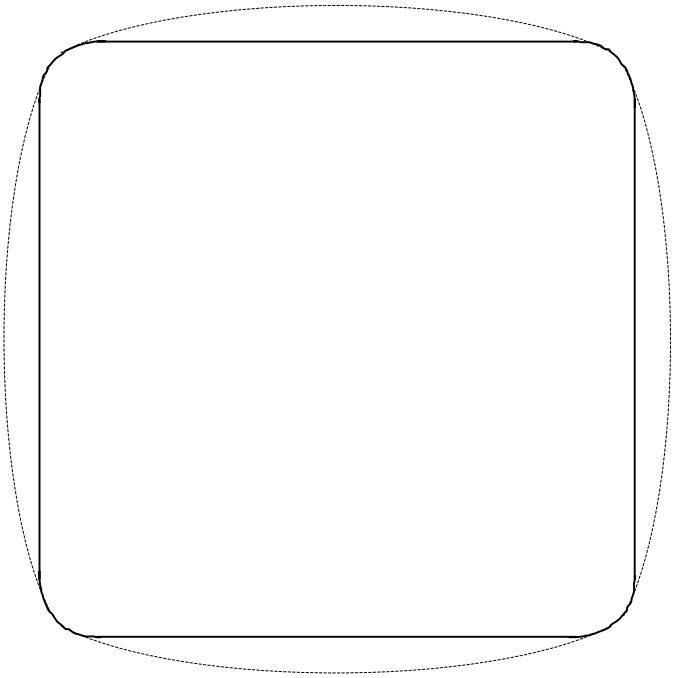

Figure 4.31. Profile of Column Cross Section Before and After Loading

To substantiate this hypothesis, consider Figure 4.32, which shows the jacket strain at the corners of 2GFRP-Rect$^{1}/_{1}$-Ti178mm-ρ1.6. Negative strains indicate compression, while positive strains indicate tension. This is one of several examples of columns on which the surface of the jacket was experiencing more than simply the effect of tension induced by the confining pressure. Similar behavior on a smaller scale may be part of the reason the strains at the corners tended to be less than the strains at the half-face position. Note that it is very unlikely that such behavior is the result of the strain gages debonding, since debonding could not cause compressive strains. Furthermore, none of the strain gages in the quarter-face and half-face positions experienced such large switchbacks in their load versus strain curves. However, small switchbacks were found at the quarter-

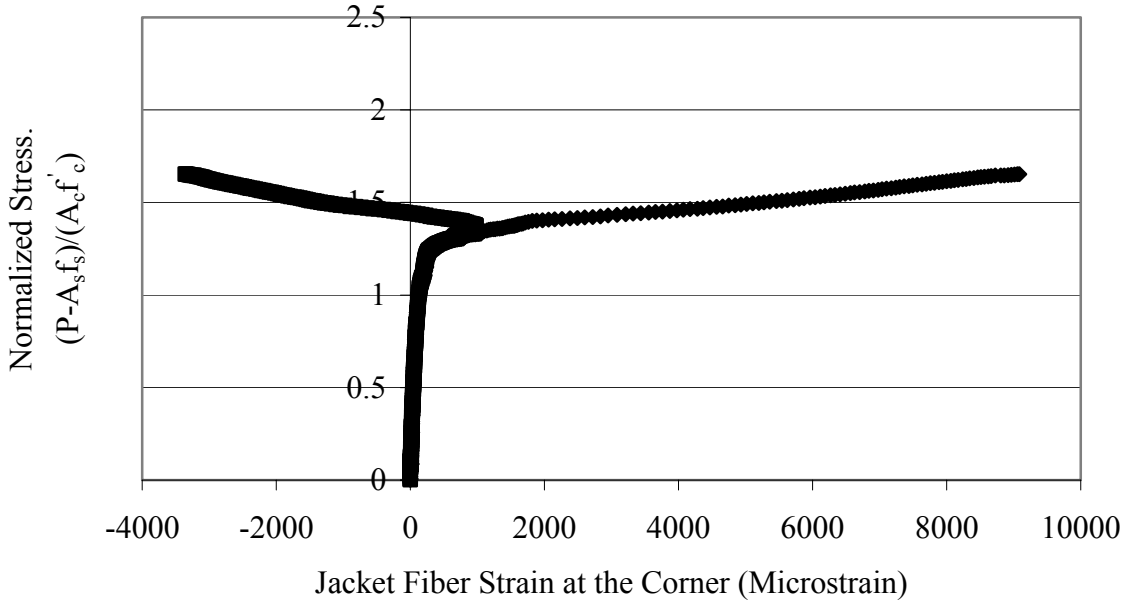

Figure 4.32. Comparison of Normalized Stress Versus Jacket Fiber Strain at the Corner (2GFRP-Rect1/1-Ti178mm-r1.6)

face position on three columns and at the half-face position on one column. No switchbacks were found in the jacket strain curves for the circular columns.

4.5.5. Circular Versus Square Cross Sections. Figure 4.33 shows the jacket strain for a circular and a square column with 1-ply CFRP jackets. The strains are very similar. Note that there is a great deal of variability among the strain readings on the circular column, even though ideally the gages should be measuring the same strain. This trend in variability among similarly positioned strain gages is common even on the rectangular specimens where, for instance, two half-face strain gages may give different readings. Figure 4.32 shows that this is certainly true for strain gage readings taken at the corner.

4.5.6. Variable Tie Spacing (2.0 Aspect Ratios). Figure 4.34 shows the jacket strain on the columns with variable tie spacings, having aspect ratios of 2.0. From the small strain readings it is clear that little of the strength of the jacket was developed before rupture. Note that the corner gage on 2CFRP-Rect2/1-Ti127mm-ρ1.6 actually shows compression. This is from a corner gage whose behavior was similar to that displayed in Figure 4.32.

4.5.7. Variable Tie Spacing (Square Cross Sections). Figure 4.35 shows the jacket strain in square cross sections with variable tie spacings. The strains are similar and give little indication of why 2CFRP-Rect1/1-Ti102mm-ρ1.6 had a smaller ultimate strength than the other two specimens (see Figure 4.15). However, since the jacket strains are virtually the same, it appears that the difference in strength was not the result of decreased confinement effectiveness brought about by the tie spacing of 102 mm.

4.5.8. Variable Jacket Thickness and Fiber Type. Figure 4.36 through Figure 4.38 display the jacket strain on square cross sections having variable CFRP, AFRP and GFRP jacket thicknesses. The GFRP and AFRP jackets having two and three

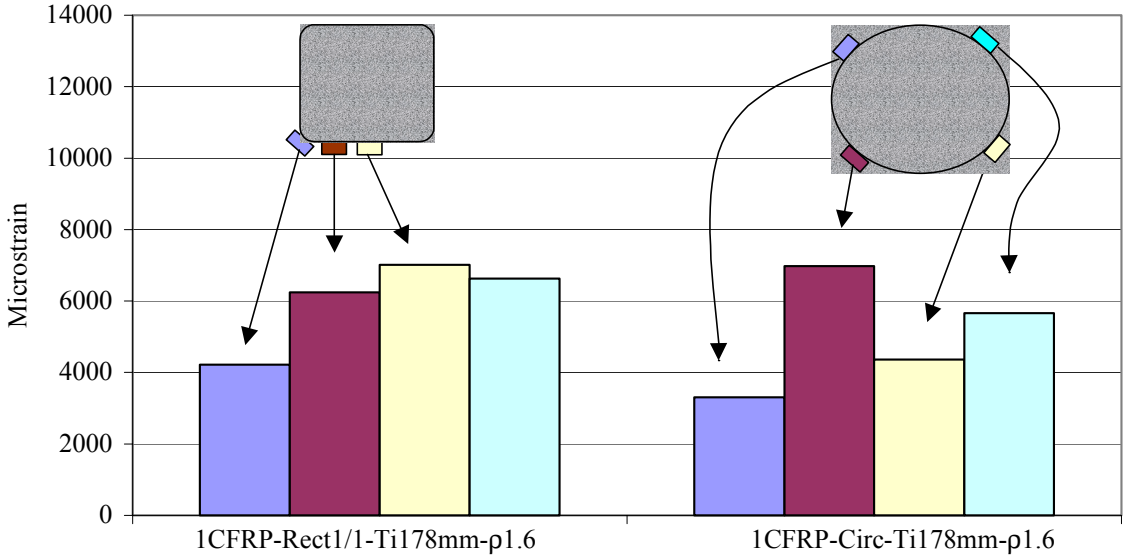

Figure 4.33. Ultimate Hoop Jacket Strain (Circular Versus Square Cross Section)

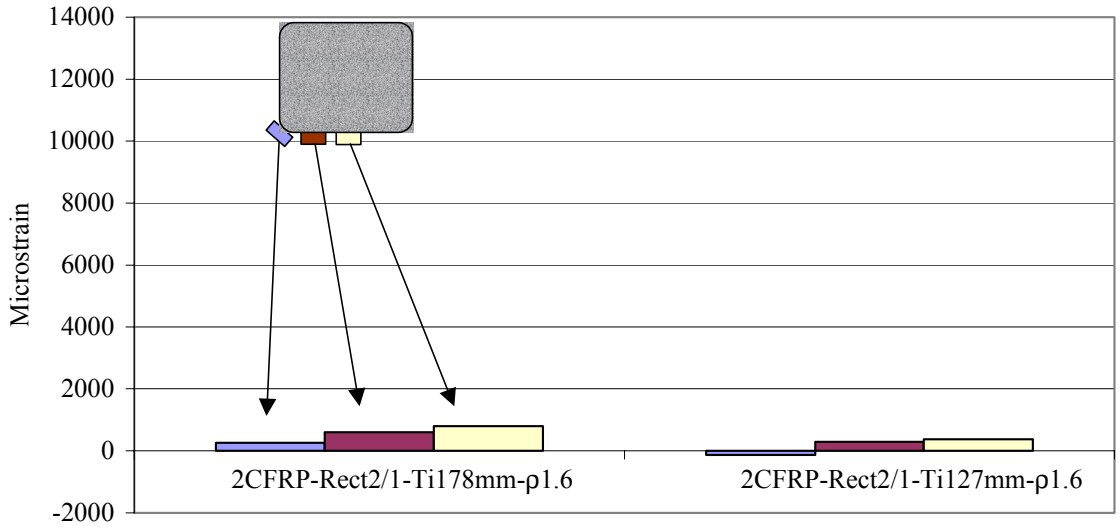

Figure 4.34. Ultimate Hoop Jacket Strain (2.0 Aspect Ratio, Variable Tie Spacing)

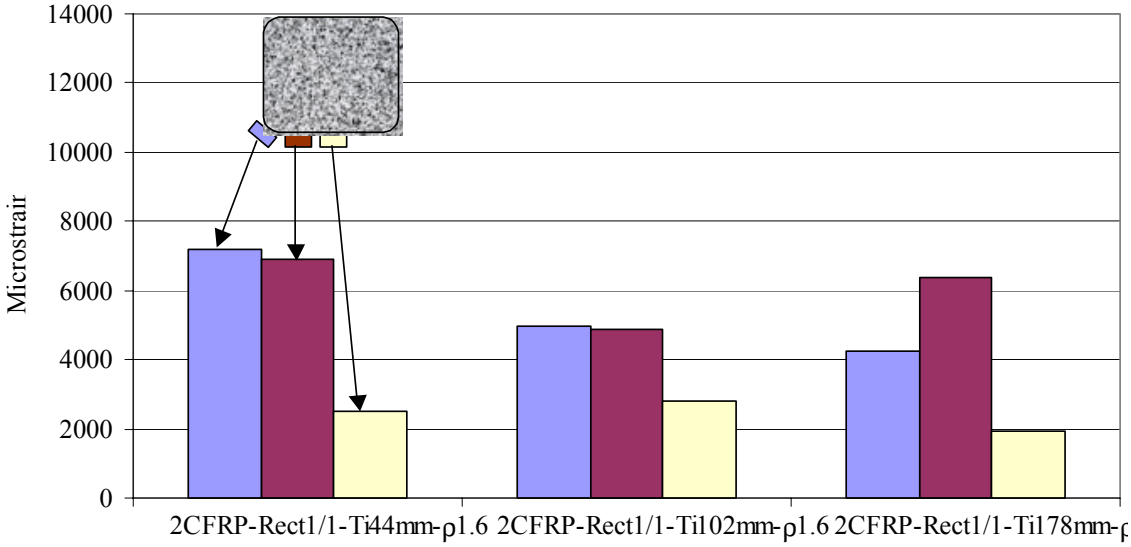

Figure 4.35. Ultimate Hoop Jacket Strain (1.0 Aspect Ratio, Variable Tie Spacing)

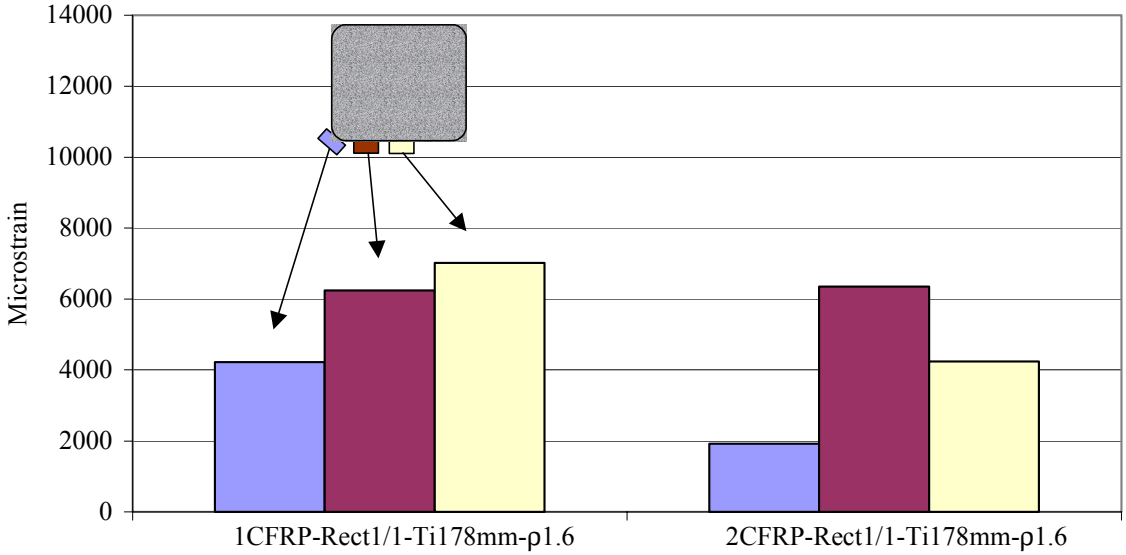

Figure 4.36. Ultimate Hoop Jacket Strain (Variable CFRP Jacket Thickness)

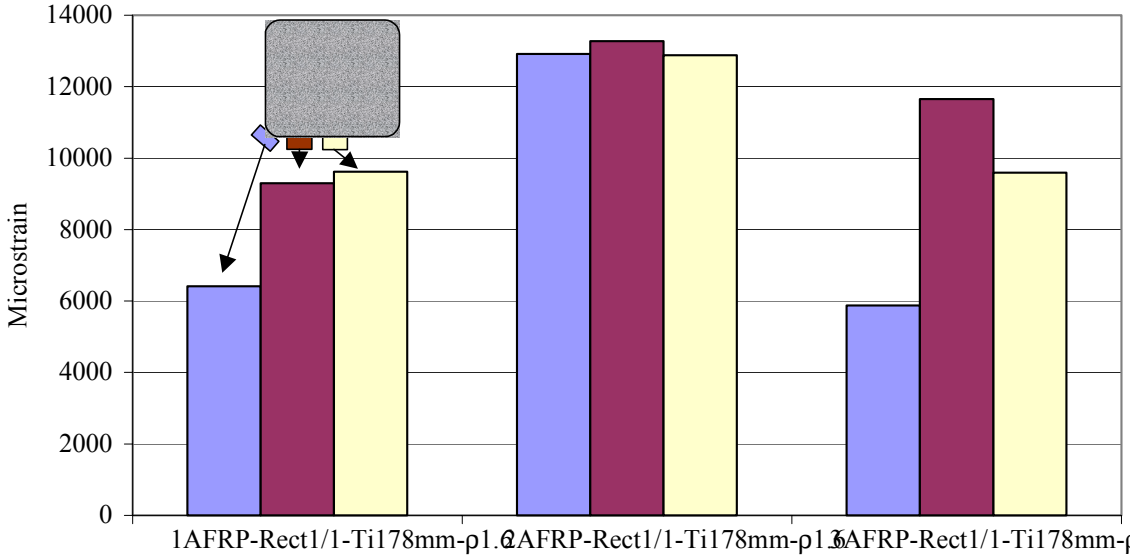

Figure 4.37. Ultimate Hoop Jacket Strain (Variable AFRP Jacket Thickness)

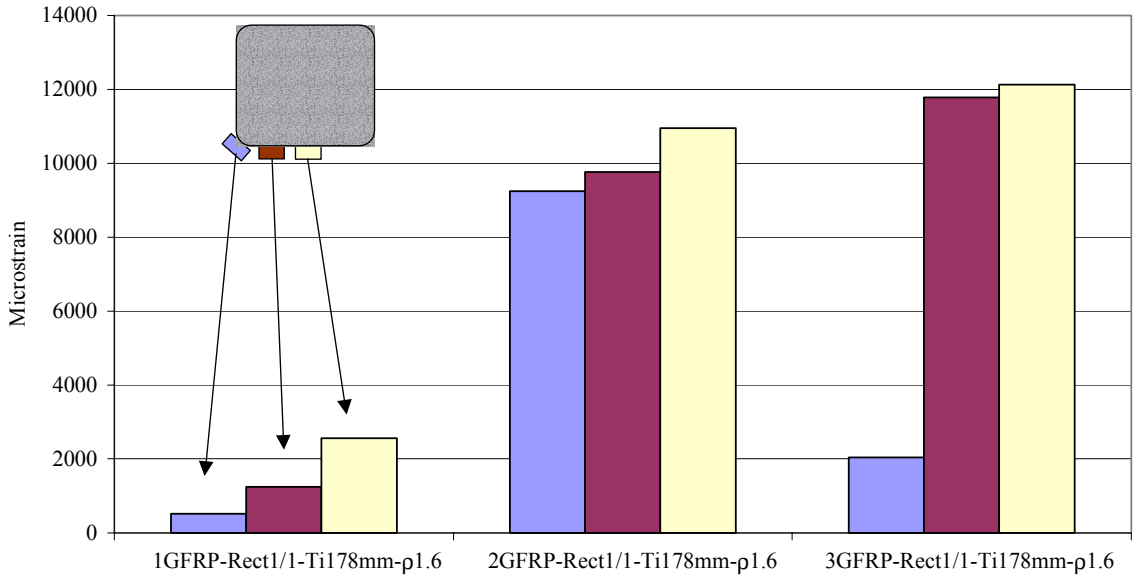

Figure 4.38. Ultimate Hoop Jacket Strain (Variable GFRP Jacket Thickness)

plies show a significant increase in strain over their respective one-ply jackets. This trend is not evident in the CFRP jackets, perhaps because, as already mentioned, the two-ply CFRP jacket failed by debonding at the lap splice. Figure 4.38 gives no strong indication of why the GFRP jackets resulted in such large normalized ultimate stresses and such large ultimate axial deformation in comparison to the two-ply and three-ply CFRP and AFRP jackets. Indeed, Figure 4.37 shows that, in comparison to the GFRP, the AFRP jackets achieved greater strain for the one-ply and two-ply specimens and only slightly smaller strains for the three-ply specimen. Recall also from Table 3.4 that the AFRP fibers are stiffer than the GFRP fibers and that the AFRP sheets can sustain a slightly greater load per sheet width than the GFRP sheets. This greater stiffness and strength coupled with the greater strains implies that the AFRP should have been applying more confinement to the cross section than the GFRP.

4.6. ANALYTICAL COMPARISON

A number of models have been proposed to predict the behavior of rectangular FRP-confined RC columns. Among them is a model proposed by Saadatmanesh et al. (1993) for use with composite belts as well as a model from Mirmiran et al. (1998) for use with FRP tubes. More recently, Chaallal and Shahawy (2000) proposed a method for predicting the capacity of rectangular columns confined by FRP jackets. In their model, the strength of the confined concrete is given as

$$f_{cc} = f_c^{'} + 3.38 f_r^{0.7} \qquad \text{Equation 4.6}$$

where $f_c^{'}$ is the unconfined cylinder strength of the concrete, and f_r is the confining pressure in ksi. This equation was taken from Mirmiran and Shahawy (1997) and developed from test data on circular columns for which f_r is uniform around the perimeter of the column. For circular columns, f_r can be shown to be

$$f_r = \left(\frac{2t_j}{D}\right)(E_j \varepsilon_j) \qquad \text{Equation 4.7}$$

where t_j is the thickness of the jacket, D is the diameter of the cross section and E_j and ε_j are the modulus of the jacket fibers and the strain in the jacket fibers, respectively.

Since the confining pressure is not uniform around the perimeter of a rectangular column, f_r is quantified through the concept of an effective area of confined concrete within the gross section (see Figure 4.39) and is taken as the larger of either $f_{r,x}$ and $f_{r,y}$, the effective lateral confining pressure in the x and y directions.

$$f_{r,x} = \left(\frac{A_e}{A_c}\right)\left(\frac{2t_j}{t_x}\right)(E_j\varepsilon_j) \qquad \text{Equation 4.8a}$$

$$f_{r,y} = \left(\frac{A_e}{A_c}\right)\left(\frac{2t_j}{t_y}\right)(E_j\varepsilon_j) \qquad \text{Equation 4.8b}$$

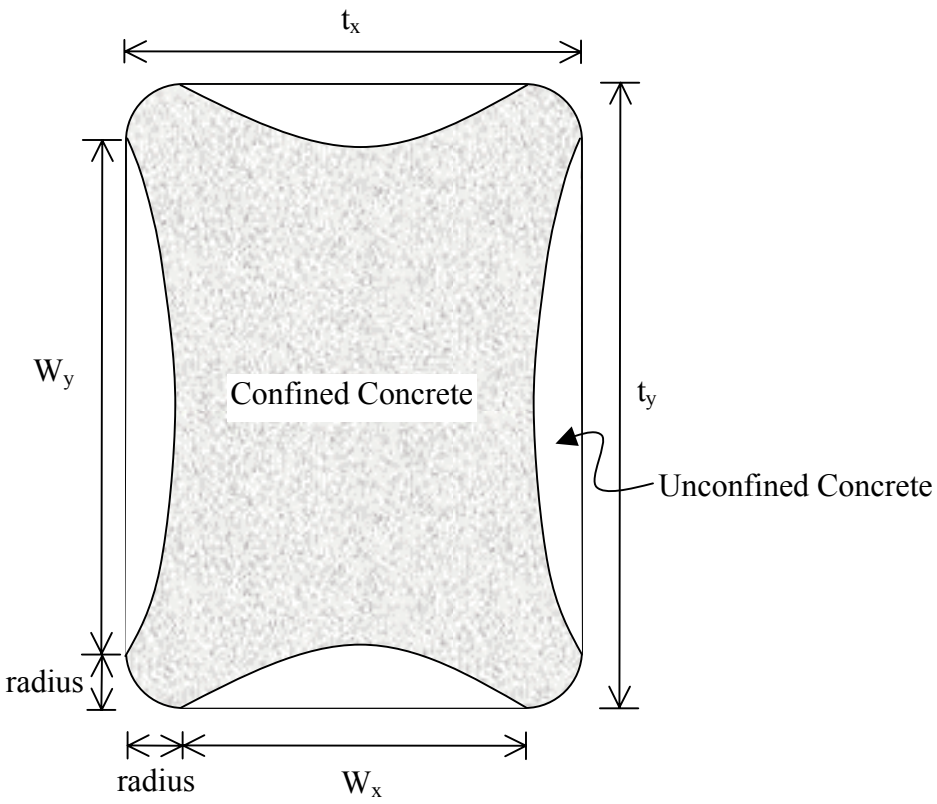

Figure 4.39. Confined and Unconfined Concrete in a Rectangular Cross Section as Depicted by Chaallal and Shahawy (2000)

In the above equations, A_c is the gross area of the cross section minus the area of longitudinal steel. A_e is the effective area of confined concrete and is given as proposed by Sheikh and Uzumeri (1980).

$$A_e = t_x t_y - \left[\frac{\left(W_x^2 + W_y^2\right)}{3}\right] - A_s \qquad \text{Equation 4.9}$$

The variables t_x, t_y, W_x and W_y are dimensions from the cross section as shown in Figure 4.39, and A_s is the area of longitudinal steel. Note the similarity of Equation 4.7 to Equation 4.8a and Equation 4.8b. They are essentially identical, except that in the circular case, the ratio of effectively confined area to total area is equal to 1.0, and the dimension of the cross section is given as D rather than t_x or t_y.

The above model has been used to predict the strength of some of the columns in the current testing program. To avoid corner effects (see Section 4.5) and to be consistent with the methodology of the originators of the model, the jacket strain, ε_j, was taken as the average of the half-face strain gage readings. The theoretical normalized strength is given in Equation 4.10.

$$\sigma_{n,ult} = \frac{f_{cc}}{f_c'} \qquad \text{Equation 4.10}$$

Table 4.1 summarizes the theoretical and experimental normalized ultimate stresses for several columns. The percent difference between the theoretical and experimental stress is calculated with respect to the experimental stress. Therefore, positive percent differences are the result of the theory overestimating the strength of the columns.

The average percent difference between the experimental and the theoretical strengths was 13.7%. However, as can be seen from Table 4.1, the agreement between the

experimental and theoretical values varied widely. The theory agrees well with the experimental data for the GFRP-wrapped specimens, but significantly overestimates the strength of the AFRP-wrapped specimens, and gives a wide range of differences for the CFRP-wrapped specimens. The model's effectiveness at predicting the strength of the GFRP-wrapped specimens may come from the fact that Equation 4.6 was originally developed from experimental data gathered from tests on GFRP-confined concrete. Another possibility is that the model may be better suited to predict the strength of columns with low concrete strengths, since the GFRP-wrapped specimens had some of the lowest cylinder strengths while the AFRP-wrapped specimens had the largest cylinder strengths (see Table 3.5).

Table 4.1. Comparison of Theoretical and Experimental Column Strengths

Column Name	Experimental $\sigma_{n,ult}$	Theoretical $\sigma_{n,ult}$	Percent Difference
1CFRP-Rect1/1-Ti178mm-ρ1.6	1.23	1.41	15.0
2CFRP-Rect1/1-Ti178mm-ρ1.6	1.33	1.38	4.0
2CFRP-Rect3/2-Ti178mm-ρ1.6	1.25	1.52	21.8
2CFRP-Rect2/1-Ti178mm-ρ1.6	1.11	1.13	1.4
1GFRP-Rect1/1-Ti178mm-ρ1.6	1.12	1.14	1.5
2GFRP-Rect1/1-Ti178mm-ρ1.6	1.66	1.78	7.2
3GFRP-Rect1/1-Ti178mm-ρ1.6	2.05	1.93	-5.7
1AFRP-Rect1/1-Ti178mm-ρ1.6	1.04	1.26	20.9
2AFRP-Rect1/1-Ti178mm-ρ1.6	1.12	1.55	38.0
3AFRP-Rect1/1-Ti178mm-ρ1.6	1.35	1.61	18.9
2CFRP-Rect1/1-Ti178mm-ρ1.6-6.4mm	1.07	1.20	12.3
2CFRP-Rect1/1-Ti178mm-ρ1.6-19mm	1.42	1.83	28.9
	Average Percent Difference = 13.7%		

4.7. SUMMARY

The results of the testing program and the observations made while performing the tests were presented in this section. The effects of the various test variables were compared with the use of several types of figures. One type of figure displayed the

ultimate normalized stress sustained by the columns. Normalizing the ultimate stress with respect to the cylinder strengths and amount of longitudinal reinforcement was necessary in order to isolate the effects of the variables under consideration. Another type of figure displayed the normalized stress in the columns as a function of the axial deformation. This figure showed that FRP-jacketed columns are typically able to sustain much more deformation than unjacketed columns. A third type of figure compared the fiber strain in the jackets at three positions: at the column corners and at two locations between the corners. It was shown that the jacket experiences little strain until the load nears the ultimate load sustainable by the column. It was also shown that, in general, the jacketed columns with the greatest improvements in strength had the largest jacket strains.

In addition to the comparison of experimental data discussed above, a theoretical model from the literature was used to predict the ultimate strength of the columns. The model appeared to be most effective at predicting the strength of GFRP-confined columns and least effective at predicting the strength of the AFRP-confined columns. The ability of the model to predict the strength of these two groups of specimens may have been influenced by the type of FRP fiber, by the unconfined concrete strengths of the specimens, or by a combination of these two variables.

5. CONCLUDING REMARKS AND FUTURE RECOMMENDATIONS

This experimental study focused on FRP jackets on non-slender RC columns under pure axial compression. The objective was to determine the effect of various experimental parameters on the confinement effectiveness of FRP jackets on rectangular columns. These experimental parameters included the cross-sectional aspect ratio (the ratio of the length of the long side of the cross section to that of the short side) of the column, the amount and type of fibers constituting the FRP jacket, the sharpness of the column corners, and the amount of longitudinal and transverse steel reinforcement in the column.

The following is a summary of the salient points regarding the effects of the test variables on the performance of the columns in this study.

- The amount of longitudinal reinforcement had little effect on the performance of 2-ply CFRP jackets on square cross sections.
- Decreasing corner sharpness led to both increased ultimate strength and increased ultimate axial deformation for 2-ply CFRP jackets on square cross sections.
- For circular columns, dual confinement from both closely spaced ties and CFRP jacketing led to a significant increase in strength over the columns with only steel or only CFRP confinement. In contrast, dual confinement on the square cross section led to strength similar to that afforded by CFRP confinement alone.
- A change in tie spacing from 102 mm to 178 mm on rectangular cross sections with a 2.0 aspect ratio led to no appreciable change in ultimate strength.
- Larger aspect ratios led to decreased strength and axial deformation.
- Increasing the thickness of CFRP, AFRP or GFRP jackets led to both increased strength and axial deformation. For square columns, GFRP jackets were observed to increase the ultimate axial strain more effectively than either AFRP or CFRP jackets. For multiple-ply jackets on square columns, GFRP was also found to be the most effective at increasing the ultimate axial stress. CFRP afforded the largest axial strength increase for single-ply jackets.

- Jackets with large fiber strains at ultimate load stages generally corresponded to the strongest, most ductile columns.
- FRP jacketing led to significant increases in axial strength even in columns with unfavorable characteristics (i.e. sharp corners or large aspect ratios). However, the increased strength was typically attained only after large axial deformations. This result leads to the conclusion that FRP jackets are most suited to impact the behavior of RC columns near their ultimate load capacity. Thus, FRP jackets can effectively increase the safety of a column by preventing its collapse under extreme loading conditions, but man not be particularly effective at greatly increasing the service loads to which a column can be subjected, since unacceptably large deformations in the column could result.

Future studies regarding the use of FRP jackets as a confinement mechanism for RC columns will compliment the results of this study and others like it. Topics for further study might include the following: the effect of the unconfined concrete strength on the ultimate strength of FRP-confined concrete, the effect of the size of the column cross section, the effect of the arrangement of the longitudinal reinforcing bars within the column cross section and the effects of various environmental conditions on the performance of the FRP jackets.

BIBLIOGRAPHY

Chaallal, O., and Shahawy, M. (2000). "Performance of fiber-reinforced polymer-wrapped reinforced concrete column under combined axial-flexural loading." *ACI Structural Journal*, 97(4), 659-668.

Chajes, M. J., Mertz, D. R., Thomson, T. A. Jr., and Farschman, C.A. (1994). "Durability of composite material reinforcement." *Infrastructure: New Materials and Methods of Repair, Proceedings of the Third Materials Engineering Conference*, ASCE, New York, New York, 598-605.

Chen, W. F. (1982). *Plasticity in Reinforced Concrete*. McGraw-Hill, Inc., New York, New York, 39-42.

Harmon, T. G., Ramakrishnan, S., and Wang, E. H. (1998). "Confined concrete subjected to uniaxial monotonic loading." *Journal of Engineering Mechanics*, ASCE, 124(12), 1303-1309.

Karbhari, V. M., and Gao, Y. (1997). "Composite jacketed concrete under uniaxial compression – verification of simple design equations." *Journal of Materials in Civil Engineering*, ASCE, 9(4), 185-193.

Liu, H., Tai, N., and Chen, C. (2000). "Compression strength of concrete columns reinforced by non-adhesive filament wound hybrid composites." *Composites - Part A: Applied Science and Manufacturing*, 31(3), 221-233.

Mallick, P. K. (1988). *Fiber-Reinforced Composites Materials, Manufacturing and Design*. Marcel Dekker, Inc., New York, New York, 1-68.

MBrace™ Composite Strengthening System Engineering Design Guidelines, Second Edition. (1998). Master Builders, Inc., Cleveland, Ohio, 4-7.

Mirmiran, A., and Shahawy, M. (1997). "Behavior of concrete columns confined by fiber composites." *Journal of Structural Engineering*, ASCE, 123(5), 583-590.

Mirmiran, A., Shahawy, M., Samaan, M., Echary, H. E., Mastrapa, J. C., and Pico, O. (1998). "Effect of column parameters on FRP-confined concrete." *Journal of Composites for Construction*, ASCE, 2(4), 175-185.

Nanni, A., and Bradford, N. M. (1995). "FRP jacketed concrete under uniaxial compression." *Construction and Building Materials*, 9(2), 115-124.

Pantelides, C.P., Gergely, J., Reaveley, L. D., and Volnyy, V. A. (1999). "Retrofit of RC bridge pier with CFRP advanced composites." *Journal of Structural Engineering*, ASCE, 125(10), 1094-1099.

Picher, F., Rochette, P., and Labossière, P. (1996). "Confinement of concrete cylinders with CFRP." *Proceedings of the 1st International Conference, Composites in Infrastructure*, H. Saadatmanesh and M. R. Ehsani, eds., University of Arizona, Tucson, Arizona, 829-841.

Saadatmanesh, H. (1997). "Extending service life of concrete and masonry structures with fiber composites." *Construction and Building Materials*, 11(5-6), 327-335.

Saadatmanesh, H., Ehsani, M. R., and Li, M. W. (1993). "Behavior of externally confined concrete columns." *Fiber Reinforced Plastic Reinforcement for Concrete Structures*, A. Nanni and C. W. Dolan, eds., SP-138, American Concrete Institute, Detroit, Michigan, 249-266.

Saafi, M., Toutanji, H. A., and Li, Z. (1999). "Behavior of concrete columns confined with fiber reinforced polymer tubes." *ACI Materials Journal*, 96(4), 500-509.

Sheikh, S. A., and Uzumeri, S.M. (1980). "Strength and ductility of tied concrete columns." *Journal of Structural Division,* ASCE, 106(5), 1079-1102.

Slattery, K. T. (1994). "Mechanistic model of the creep-rupture process in filamentary composites." *Infrastructure: New Materials and Methods of Repair, Proceedings, Third Materials Engineering Conference*, ASCE, New York, New York, 215-222.

Toutanji, H. A. (1999). "Stress-strain characteristics of concrete columns externally confined with advanced fiber composite sheets." *ACI Materials Journal*, 96(3), 397-404.

Xiao, Y., and Wu, H. (2000). "Compressive behavior of concrete confined by carbon fiber composite jackets." *Journal of Materials in Civil Engineering*, ASCE, 12(2), 139-146.

Xiao, Y., Wu, H., and Martin, G. R. (1999). "Prefabricated composite jacketing of RC columns for enhanced shear strength." *Journal of Structural Engineering*, ASCE, 125(3), 255-264.